

CERN-EP-2017-015
25 January 2017

Energy dependence of forward-rapidity J/ψ and $\psi(2S)$ production in pp collisions at the LHC

ALICE Collaboration*

Abstract

We present results on transverse momentum (p_T) and rapidity (y) differential production cross sections, mean transverse momentum and mean transverse momentum square of inclusive J/ψ and $\psi(2S)$ at forward rapidity ($2.5 < y < 4$) as well as $\psi(2S)$ -to- J/ψ cross section ratios. These quantities are measured in pp collisions at center of mass energies $\sqrt{s} = 5.02$ and 13 TeV with the ALICE detector. Both charmonium states are reconstructed in the dimuon decay channel, using the muon spectrometer. A comprehensive comparison to inclusive charmonium cross sections measured at $\sqrt{s} = 2.76, 7$ and 8 TeV is performed. A comparison to non-relativistic quantum chromodynamics and fixed-order next-to-leading logarithm calculations, which describe prompt and non-prompt charmonium production respectively, is also presented. A good description of the data is obtained over the full p_T range, provided that both contributions are summed. In particular, it is found that for $p_T > 15$ GeV/c the non-prompt contribution reaches up to 50% of the total charmonium yield.

arXiv:1702.00557v2 [hep-ex] 6 Jul 2017

© 2017 CERN for the benefit of the ALICE Collaboration.

Reproduction of this article or parts of it is allowed as specified in the CC-BY-4.0 license.

*See Appendix A for the list of collaboration members

1 Introduction

Charmonia, such as J/ψ and $\psi(2S)$, are bound states of a charm and anti-charm quark ($c\bar{c}$). At LHC energies, their hadronic production results mostly from the hard scattering of two gluons into a $c\bar{c}$ pair followed by the evolution of this pair into a charmonium state. Charmonium measurements in pp collisions are essential to the investigation of their production mechanisms. They also provide a baseline for proton-nucleus and nucleus-nucleus results which in turn are used to quantify the properties of the quark-gluon plasma [1, 2].

Mainly three theoretical approaches are used to describe the hadronic production of charmonium: the Color Evaporation Model (CEM) [3, 4], the Color Singlet Model (CSM) [5] and the Non-Relativistic Quantum Chromo-Dynamics model (NRQCD) [6]. These approaches differ mainly in the treatment of the evolution of the heavy-quark pair into a bound state. In the CEM, the production cross section of a given charmonium is proportional to the $c\bar{c}$ cross section, integrated between the mass of the charmonium and twice the mass of the lightest D meson, with the proportionality factor being independent of the charmonium transverse momentum p_T , rapidity y and of the collision center of mass energy \sqrt{s} . In the CSM, perturbative QCD is used to describe the $c\bar{c}$ production with the same quantum numbers as the final-state meson. In particular, only color-singlet (CS) $c\bar{c}$ pairs are considered. Finally, in the NRQCD framework charmonium can be formed from a $c\bar{c}$ pair produced either in a CS or in a color-octet (CO) state. The color neutralization of the CO state is treated as a non-perturbative process. For a given order in α_s , it is expanded in powers of the relative velocity between the two charm quarks and parametrized using universal Long Distance Matrix Elements (LDME) which are fitted to the data. The predictive power of NRQCD calculations is tested by fitting the LDME to a subset of the data and comparing cross sections calculated with these LDME to measurements performed at different energies. It is therefore crucial to confront these models to as many measurements as possible, over a wide range of p_T , y and \sqrt{s} , and with as many different charmonium states as possible. The comparison can also be extended to observables other than cross sections, such as charmonium polarization [7–9].

In this paper we present results on the production cross sections of inclusive J/ψ and $\psi(2S)$ at forward rapidity ($2.5 < y < 4$) measured in pp collisions at center of mass energies $\sqrt{s} = 13$ and 5.02 TeV. For J/ψ at $\sqrt{s} = 5.02$ TeV, the p_T -differential cross sections have been published in [10] while the y -differential cross sections are presented here for the first time.

The J/ψ and $\psi(2S)$ are measured in the dimuon decay channel. The inclusive differential cross sections are obtained as a function of p_T and y over the ranges $0 < p_T < 30$ GeV/ c for J/ψ at $\sqrt{s} = 13$ TeV, $0 < p_T < 12$ GeV/ c for J/ψ at $\sqrt{s} = 5.02$ TeV and $0 < p_T < 16$ GeV/ c for $\psi(2S)$ at $\sqrt{s} = 13$ TeV. At $\sqrt{s} = 5.02$ TeV only the p_T -integrated $\psi(2S)$ cross section is measured due to the limited integrated luminosity. The J/ψ result at $\sqrt{s} = 13$ TeV extends significantly the p_T reach of measurements performed in a similar rapidity range by LHCb [11]. The J/ψ result at $\sqrt{s} = 5.02$ TeV and the $\psi(2S)$ results at both \sqrt{s} are the first at this rapidity. The inclusive $\psi(2S)$ -to- J/ψ cross section ratios as a function of both p_T and y are also presented. These results are compared to similar measurements performed at $\sqrt{s} = 2.76$ [12], 7 [13] and 8 TeV [14]. These comparisons allow studying the variations of quantities such as the mean transverse momentum $\langle p_T \rangle$, mean transverse momentum square $\langle p_T^2 \rangle$ and the p_T -integrated cross section as a function of \sqrt{s} . Put together, these measurements constitute a stringent test for models of charmonium production. In particular, an extensive comparison of the J/ψ and $\psi(2S)$ cross sections at all available collision energies to the calculations from two NRQCD groups is presented towards the end of the paper (Sec. 4). In addition, the p_T -integrated J/ψ cross section as a function of \sqrt{s} is also compared to a CEM calculation. No comparison to the CSM is performed since complete calculations are not available at these energies beside the ones published in [13, 15].

All cross sections reported in this paper are inclusive and contain, on top of the direct production of the charmonium, a contribution from the decay of heavier charmonium states as well as contributions

from the decay of long-lived beauty flavored hadrons (b -hadrons). The first two contributions (direct production and decay from heavier charmonium states) are commonly called prompt, whereas the contribution from b -hadron decays is called non-prompt because of the large mean proper decay length of these hadrons ($\sim 500 \mu\text{m}$).

The paper is organized as follows: the ALICE apparatus and the data samples used for this analysis are described in Sec. 2, the analysis procedure is discussed in Sec. 3 while the results are presented and compared to measurements at different \sqrt{s} as well as to models in Sec. 4.

2 Apparatus and data samples

The ALICE detector is described in detail in [16, 17]. In this section, we introduce the detector subsystems relevant to the present analysis: the muon spectrometer, the Silicon Pixel Detector (SPD), the V0 scintillator hodoscopes and the T0 Cherenkov detectors.

The muon spectrometer [18] allows the detection and characterization of muons in the pseudorapidity range $-4 < \eta < -2.5$ ¹. It consists of a ten-interaction-lengths front absorber followed by a 3 T-m dipole magnet coupled to a system of tracking (MCH) and triggering (MTR) devices. The front absorber is placed between 0.9 and 5 m from the Interaction Point (IP) and filters out hadrons and low-momentum muons emitted at forward rapidity. Tracking in the MCH is performed using 5 stations, each one consisting of two planes of cathode pad chambers positioned between 5.2 and 14.4 m from the IP. The MTR is positioned downstream of a 1.2 m thick iron wall which absorbs the remaining hadrons that escape the front absorber as well as low-momentum muons. It is composed of two stations equipped with two planes of resistive plate chambers each placed at 16.1 and 17.1 m from the IP. A conical absorber ($\theta < 2^\circ$) protects the muon spectrometer against secondary particles produced mainly by large- η primary particles interacting with the beam pipe throughout its full length. Finally, a rear absorber located downstream of the spectrometer protects the MTR from the background generated by beam-gas interactions.

The SPD is used to reconstruct the primary vertex of the collision. It is a cylindrically-shaped silicon pixel tracker and corresponds to the two innermost layers of the Inner Tracking System (ITS) [19]. These two layers surround the beam pipe at average radii of 3.9 and 7.6 cm and cover the pseudorapidity intervals $|\eta| < 2$ and $|\eta| < 1.4$, respectively.

The V0 hodoscopes [20] consist of two scintillator arrays positioned on each side of the IP at $z = -90$ and 340 cm and covering the η range $-3.7 < \eta < -1.7$ and $2.8 < \eta < 5.1$ respectively. They are used for online triggering and to reject beam-gas events by means of offline timing cuts together with the T0 detectors.

Finally, the T0 detectors [21] are used for the luminosity determination. They consist of two arrays of quartz Cherenkov counters placed on both sides of the IP covering the η ranges $-3.3 < \eta < -3$ and $4.6 < \eta < 4.9$.

The data used for this paper were collected in 2015. They correspond to pp collisions at $\sqrt{s} = 13$ and 5.02 TeV. The data at $\sqrt{s} = 13$ TeV are divided into several sub-periods corresponding to different beam conditions and leading to different pile-up rates. The pile-up rate, defined as the probability that one recorded event contains two or more collisions, reaches up to 25% in the muon spectrometer for beams with the highest luminosity. The data at $\sqrt{s} = 5.02$ TeV were collected during the 5 days immediately after the $\sqrt{s} = 13$ TeV campaign. During this period the pile-up rate was stable and below 2.5%.

Events used for this analysis were collected using a dimuon trigger which requires that two muons of

¹We note that the ALICE reference frame defines the positive z direction along the counter-clockwise beam direction, resulting in a negative pseudorapidity range for detectors like the muon spectrometer. However, due to the symmetry of pp collisions, the rapidity is kept positive when presenting results.

opposite sign are detected in the MTR in coincidence with the detection of a signal in each side of the V0. In addition, the transverse momentum p_T^{trig} of each muon, evaluated online, is required to pass a threshold of 0.5 GeV/c (1 GeV/c) for the data taking at $\sqrt{s} = 5.02$ (13) TeV in order to reject soft muons from π and K decays and to limit the trigger rate when the instantaneous luminosity is high. This threshold is defined as the p_T value for which the single muon trigger efficiency reaches 50% [22].

The data samples available after the event selection described above correspond to an integrated luminosity $L_{\text{int}} = 3.19 \pm 0.11 \text{ pb}^{-1}$ and $L_{\text{int}} = 106.3 \pm 2.2 \text{ nb}^{-1}$ for $\sqrt{s} = 13 \text{ TeV}$ and $\sqrt{s} = 5.02 \text{ TeV}$ respectively. These integrated luminosities are measured following the procedure described in [23] for the data at $\sqrt{s} = 13 \text{ TeV}$ and in [24] for those at $\sqrt{s} = 5.02 \text{ TeV}$. The systematic uncertainty on these quantities contains contributions from the measurement of the T0 trigger cross section using the Van der Meer scan technique [25] and the stability of the T0 trigger during data taking. The quadratic sum of these contributions amounts to 3.4% at $\sqrt{s} = 13 \text{ TeV}$ and 2.1% at $\sqrt{s} = 5.02 \text{ TeV}$.

3 Analysis

The differential production cross section for a charmonium state ψ in a given p_T and y interval is:

$$\frac{d^2\sigma_\psi}{dp_T dy} = \frac{1}{\Delta p_T \Delta y} \frac{1}{L_{\text{int}}} \frac{N_\psi(p_T, y)}{\text{BR}_{\psi \rightarrow \mu^+ \mu^-} A\mathcal{E}(p_T, y)}, \quad (1)$$

where $\text{BR}_{\psi \rightarrow \mu^+ \mu^-}$ is the branching ratio of the charmonium state ψ into a pair of muons ($5.96 \pm 0.03\%$ for J/ψ and $0.79 \pm 0.09\%$ for $\psi(2S)$) [26], Δp_T and Δy are the widths of the p_T and y interval under consideration, $N_\psi(p_T, y)$ is the number of charmonia measured in this interval, $A\mathcal{E}(p_T, y)$ are the corresponding acceptance and efficiency corrections and L_{int} is the integrated luminosity of the data sample. The large pile-up rates mentioned in Sec. 2 for the $\sqrt{s} = 13 \text{ TeV}$ data sample are accounted for in the calculation of L_{int} [23].

3.1 Track selection

The number of charmonia in a given p_T and y interval is obtained by forming pairs of opposite-sign muon tracks detected in the muon spectrometer and by calculating the invariant mass of these pairs, $m_{\mu\mu}$. The resulting distribution is then fitted with several functions that account for both the charmonium signal and the background.

The procedure used to reconstruct muon candidates in the muon spectrometer is described in [18]. Once muon candidates are reconstructed, additional offline criteria are applied in order to improve the quality of the dimuon sample and the signal-to-background (S/B) ratio.

Tracks reconstructed in the MCH are required to match a track in the MTR which satisfies the single muon trigger condition mentioned in Sec. 2. Each muon candidate is required to have a pseudorapidity in the interval $-4 < \eta < -2.5$ in order to match the acceptance of the muon spectrometer. Finally, a cut on the transverse coordinate of the muon (R_{abs}) measured at the end of the front absorber, $17.5 < R_{\text{abs}} < 89 \text{ cm}$, ensures that muons emitted at small angles and passing through the high density section of the front absorber are rejected.

These selection criteria remove most of the background tracks consisting of hadrons escaping from or produced in the front absorber, low- p_T muons from π and K decays, secondary muons produced in the front absorber and fake tracks. They improve the S/B ratio by up to 30% for the J/ψ and by a factor 2 for $\psi(2S)$.

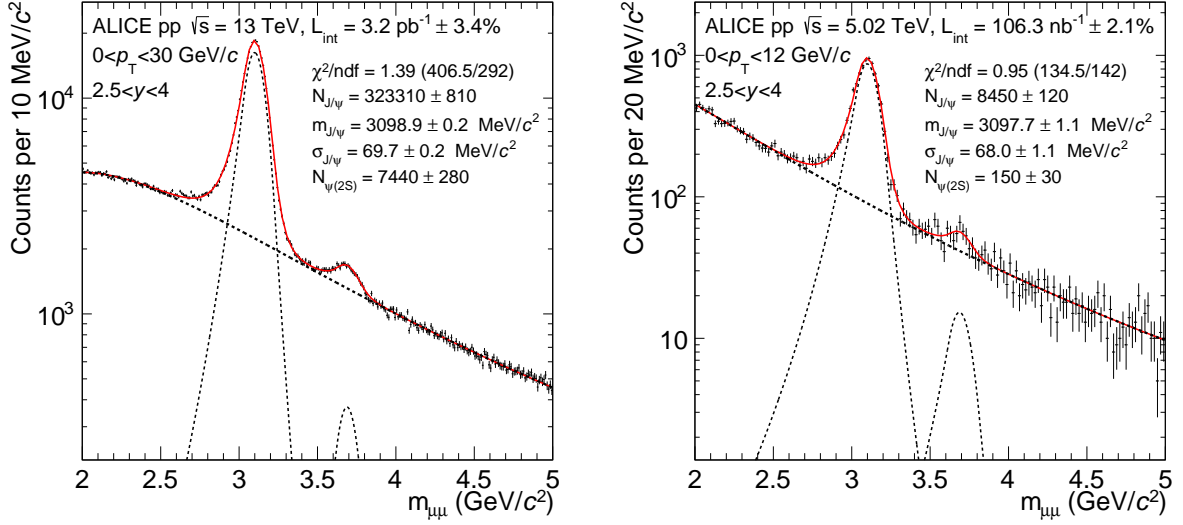


Fig. 1: Example of fit to the opposite-sign dimuon invariant mass distributions in pp collisions at $\sqrt{s} = 13$ TeV (left) and 5.02 TeV (right). Dashed lines correspond to either signal or background functions, whereas the solid line corresponds to the sum of the signal and background functions.

3.2 Signal extraction

In each dimuon p_T and y interval, several fits to the invariant mass distribution are performed over different invariant mass ranges and using various fitting functions in order to obtain the number of J/ψ and $\psi(2S)$ and to evaluate the corresponding systematic uncertainty. In all cases, the fit function consists of a background to which two signal functions are added, one for the J/ψ and one for the $\psi(2S)$.

At $\sqrt{s} = 13$ TeV, the fits are performed over the invariant mass ranges $2.2 < m_{\mu\mu} < 4.5$ GeV/c^2 and $2 < m_{\mu\mu} < 5$ GeV/c^2 . The background is described by either a pseudo-Gaussian function whose width varies linearly with the invariant mass or the product of a fourth-order polynomial and an exponential form. The J/ψ and $\psi(2S)$ signals are described by the sum of either two Crystal Ball or two pseudo-Gaussian functions [27]. These two signal functions consist of a Gaussian core with tails added on the sides that fall off slower than a Gaussian function. In most p_T and y intervals the parameters entering the definition of these tails cannot be left free in the fit due to the poor S/B ratio in the corresponding invariant mass region. They are instead fixed either to the values obtained from Monte Carlo (MC) simulations described in Sec. 3.3, or to those obtained when fitting the measured p_T - and y -integrated invariant mass distribution with these parameters left free. For the J/ψ , the position, width and normalization of the signal are free parameters of the fit. For the $\psi(2S)$ only the normalization is free, whereas the position and width are bound to those of the J/ψ following the same procedure as in [14]. Finally, in all fits the background parameters are left free.

An identical approach is used at $\sqrt{s} = 5.02$ TeV, albeit with different invariant mass fitting ranges ($1.7 < m_{\mu\mu} < 4.8$ GeV/c^2 and $2 < m_{\mu\mu} < 4.4$ GeV/c^2) and a different set of background functions (a pseudo-Gaussian function or the ratio between a first- and a second-order polynomial function). For the signal the tails parameters are either fixed to those obtained in MC or taken from the $\sqrt{s} = 13$ TeV analysis.

The number of charmonia measured in a given p_T and y interval and the corresponding statistical uncertainty are taken as the mean of the values and uncertainties obtained from all the fits performed in this interval. The root mean square of these values is used as a systematic uncertainty.

Examples of fits to the p_T - and y -integrated invariant mass distributions are shown in Fig. 1, at $\sqrt{s} = 13$ (left) and 5.02 TeV (right). About 331×10^3 J/ψ and 8.1×10^3 $\psi(2S)$ are measured at $\sqrt{s} = 13$ TeV

whereas about 8.6×10^3 J/ψ and 160 $\psi(2S)$ are measured at $\sqrt{s} = 5.02$ TeV. Corresponding S/B ratios, evaluated within three standard deviations with respect to the charmonium pole mass, are 3.4 (4.5) for J/ψ and 0.15 (0.18) for $\psi(2S)$ at $\sqrt{s} = 13$ (5.02) TeV.

3.3 Acceptance and efficiency corrections

Acceptance and efficiency corrections are obtained using MC simulations by computing the ratio between the number of charmonia reconstructed in the muon spectrometer and the number of generated charmonia in the same p_T and y interval. Independent simulations are performed for J/ψ and $\psi(2S)$ and for each collision energy. Charmonia are generated using input p_T and y distributions obtained iteratively from the data. They are decayed into two muons using EVTGEN [28] and PHOTOS [29] to properly account for the possible emission of accompanying radiative photons. It is assumed that both J/ψ and $\psi(2S)$ are unpolarized consistently with the small longitudinal values reported in [7–9] and accounting for further dilution coming from non-prompt charmonia. The decay muons are tracked through a GEANT3 [30] model of the apparatus that includes a realistic description of the detectors and their performance during data taking. Track reconstruction and signal extraction are performed from the simulated hits generated in the detector using the same procedure and selection criteria as those used for the data.

The systematic uncertainty on acceptance and efficiency corrections contains the following contributions: (i) the parametrization of the input p_T and y distributions, (ii) the uncertainty on the tracking efficiency in the MCH, (iii) the uncertainty on the MTR efficiency and (iv) the matching between tracks reconstructed in the MCH and tracks in the MTR.

For the parametrization of the MC input distributions, two sources of systematic uncertainty are considered: the correlations between p_T and y (more explicitly, the fact that the p_T distribution of a given charmonium state varies with the rapidity interval in which it is measured [11]) and the effect of finite statistics in the data used to parametrize these distributions. At $\sqrt{s} = 5.02$ TeV, both contributions are evaluated by varying the input p_T and y distributions within limits that correspond to these effects and re-calculating the $A\mathcal{E}$ corrections in each case as done in [13]. This corresponds to a variation of the input yields of at most 15% as a function of y and 50% as a function of p_T . For J/ψ measurements at $\sqrt{s} = 13$ TeV a slightly different approach is adopted in order to further reduce the sensitivity of the simulations to the input p_T and y distributions. It consists in evaluating the acceptance and efficiency corrections in small 2-dimensional bins of y and p_T . These corrections are then applied on a dimuon pair-by-pair basis when forming the invariant mass distribution rather than applying them on the total number of measured charmonia in a given (larger) p_T and y interval. For each pair the corrections that match its p_T and y are used, thus making the resulting $A\mathcal{E}$ -corrected invariant mass distribution largely independent from the p_T and y distributions used as input to the simulations. For $\psi(2S)$ this improved procedure is not applied because the uncertainties on the measurement are dominated by statistics and the same method as for J/ψ at $\sqrt{s} = 5.02$ TeV is used instead.

The other three sources of systematic uncertainty (tracking efficiency in the MCH, MTR efficiency, and matching between MTR and MCH tracks) are evaluated using the same procedure as in [13], by comparing data and MC at the single muon level and propagating the observed differences to the dimuon case.

3.4 Summary of the systematic uncertainties

Table 1 gives a summary of the relative systematic uncertainties on the charmonium cross sections measured at $\sqrt{s} = 13$ and $\sqrt{s} = 5.02$ TeV. The total systematic uncertainty is the quadratic sum of all the sources listed in this table. The uncertainty on the branching ratio is fully correlated between all measurements of a given state. The uncertainty on the integrated luminosity is fully correlated between measurements performed at the same \sqrt{s} and considered as uncorrelated from one \sqrt{s} to the other. The

uncertainty on the signal extraction is considered as uncorrelated as a function of p_T , y and \sqrt{s} , but partially correlated between J/ψ and $\psi(2S)$. Finally, all other sources of uncertainty are considered as partially correlated across measurements at the same energy and uncorrelated from one energy to the other.

The systematic uncertainties on the MTR and MCH efficiencies are significantly smaller for the data at $\sqrt{s} = 5.02$ TeV than at $\sqrt{s} = 13$ TeV. This is due to the fact that the corresponding data taking period being very short, the detector conditions were more stable and therefore simpler to describe in the simulation.

Source	$\sqrt{s} = 13$ TeV		$\sqrt{s} = 5.02$ TeV	
	J/ψ (%)	$\psi(2S)$ (%)	J/ψ (%)	$\psi(2S)$ (%)
Branching ratio	0.6	11	0.6	11
Luminosity	3.4	3.4	2.1	2.1
Signal extraction	3 (3 – 8)	5 (5 – 9)	3 (1.5 – 10)	8
MC input	0.5 (0.5 – 1.5)	1 (0.5 – 4)	2 (0.5 – 2.5)	2.5
MCH efficiency	4	4	1	1
MTR efficiency	4 (1.5 – 4)	4 (1.5 – 4)	2 (1.5 – 2)	2
Matching	1	1	1	1

Table 1: Relative systematic uncertainties associated to the J/ψ and $\psi(2S)$ cross section measurements at $\sqrt{s} = 13$ and 5.02 TeV. Values in parenthesis correspond to the minimum and maximum values as a function of p_T and y . For $\psi(2S)$ at $\sqrt{s} = 5.02$ TeV, only the p_T -integrated values are reported.

4 Results

4.1 Cross sections and cross section ratios at $\sqrt{s} = 13$ and 5.02 TeV

Fig. 2 summarizes the inclusive J/ψ and $\psi(2S)$ cross sections measured by ALICE in pp collisions at $\sqrt{s} = 13$ TeV as a function of the charmonium p_T (left column) and y (right column). The top row shows the J/ψ cross sections, middle row the $\psi(2S)$ cross sections and bottom row the $\psi(2S)$ -to- J/ψ cross section ratios. In all figures except Figs. 5 and 6, systematic uncertainties are represented by boxes, while vertical lines are used for statistical uncertainties.

The J/ψ production cross sections as a function of p_T and y are compared to measurements published by LHCb [11] at the same energy. The quoted LHCb values correspond to the sum of the prompt and the non-prompt contributions to the J/ψ production. For the comparison as a function of p_T , the provided double-differential (p_T and y) cross sections are summed to match ALICE y coverage. The measurements of the two experiments are consistent within 1σ of their uncertainties. The ALICE measurement extends the p_T reach from 14 GeV/ c to 30 GeV/ c with respect to the LHCb results. For the $\psi(2S)$ measurement, no comparisons are performed as this is the only measurement available to date at this energy and y range.

Systematic uncertainties on the signal extraction are reduced when forming the $\psi(2S)$ -to- J/ψ cross section ratios shown in the bottom panels of Fig. 2 due to correlations between the numerator and the denominator. All other sources of systematic uncertainties cancel except for the uncertainties on the MC input p_T and y parametrizations. Measured ratios show a steady increase as a function of p_T and little or no dependence on y within uncertainties. This is also the case at lower \sqrt{s} as it will be discussed in the next section.

Fig. 3 shows the inclusive J/ψ production cross section measurements performed by ALICE in pp col-

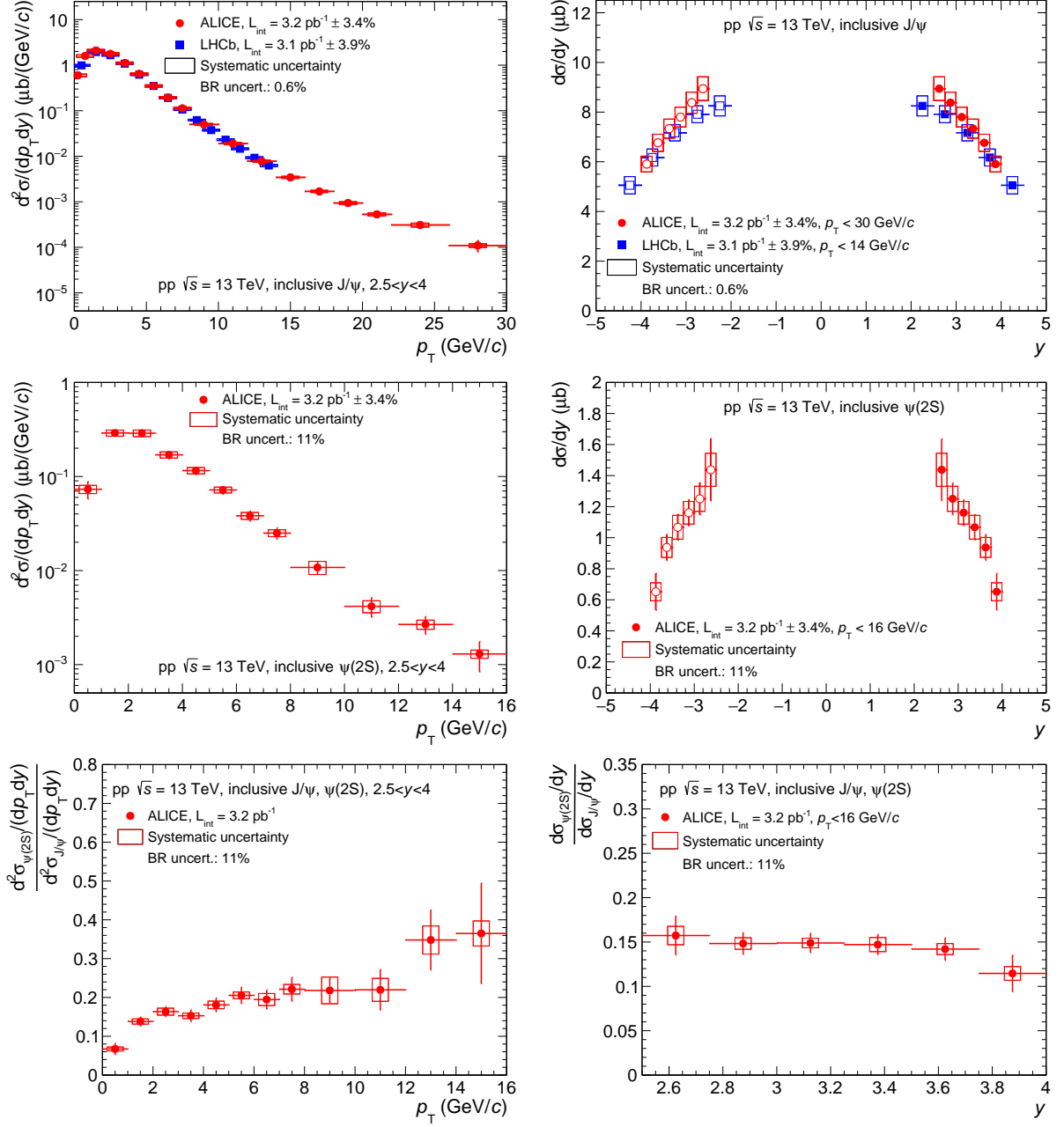


Fig. 2: (color online). Inclusive J/ψ cross sections (top), $\psi(2S)$ cross sections (middle) and $\psi(2S)$ -to- J/ψ cross section ratios (bottom) as a function of p_T (left) and y (right) in pp collisions at $\sqrt{s} = 13$ TeV. J/ψ cross sections are compared to LHCb measurements at the same \sqrt{s} [11]. Open symbols are the reflection of the positive- y measurements with respect to $y = 0$.

lisions at $\sqrt{s} = 5.02$ TeV as a function of p_T (left) and y (right). The p_T -differential cross sections are published in [10] and serve as a reference for the J/ψ nuclear modification factors in Pb–Pb collisions at the same \sqrt{s} . The y -differential cross sections are new to this analysis. Due to the limited integrated luminosity, only the p_T - and y -integrated $\psi(2S)$ cross section is measured using this data sample. It is discussed in the next section.

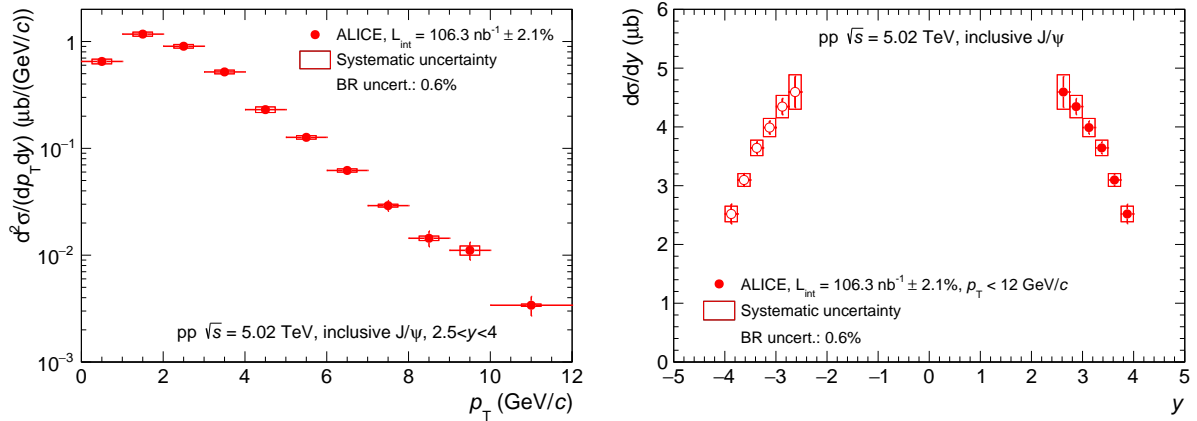


Fig. 3: Inclusive J/ψ cross sections as function of p_T (left) and y (right) in pp collisions at $\sqrt{s} = 5.02$ TeV. Open symbols are the reflection of the positive- y measurements with respect to $y = 0$.

4.2 Comparison to measurements at $\sqrt{s} = 2.76, 7$ and 8 TeV

In Fig. 4, the cross sections and cross section ratios presented in the previous section are compared to other forward- y measurements in pp collisions at $\sqrt{s} = 2.76$ [12], 7 [13] and 8 TeV [14]. We note that the integrated luminosity used for each measurement increases almost systematically with increasing \sqrt{s} , starting from 19.9 nb^{-1} at $\sqrt{s} = 2.76$ TeV up to 3.2 pb^{-1} at $\sqrt{s} = 13$ TeV. This, combined with the fact that the charmonium cross-section also increases with \sqrt{s} , has allowed to reach increasingly higher values of p_T for both J/ψ and $\psi(2S)$ measurements. For the J/ψ this corresponds to an increase of the p_T reach from $8 \text{ GeV}/c$ at $\sqrt{s} = 2.76$ TeV up to $30 \text{ GeV}/c$ at $\sqrt{s} = 13$ TeV. For the $\psi(2S)$ the corresponding increase goes from $12 \text{ GeV}/c$ at $\sqrt{s} = 7$ TeV to $16 \text{ GeV}/c$ at $\sqrt{s} = 13$ TeV.

The J/ψ p_T -differential cross section measurements shown in the top-left panel of Fig. 4 indicate a hardening of the spectra with increasing \sqrt{s} . Also, for $\sqrt{s} \geq 7$ TeV, a change in the slope of the p_T -differential cross section is visible for $p_T > 10 \text{ GeV}/c$. This change in slope is attributed to the onset of the contribution from non-prompt J/ψ to the inclusive cross section as it will be discussed in Sec. 4.3.

The corresponding $\psi(2S)$ differential cross section measurements are shown in the middle panels of Fig. 4. The smaller cross sections with respect to J/ψ result in a smaller p_T reach as well as larger statistical uncertainties as a function of both p_T (left panel) and y (right panel).

In the bottom panels of Fig. 4 the measured $\psi(2S)$ -to- J/ψ cross section ratios are compared as a function of p_T (left) and y (right) for pp collisions at $\sqrt{s} = 7, 8$ and 13 TeV. No significant change neither in shape nor magnitude of the ratio is observed among the three energies within the current uncertainties.

To better quantify the hardening of the J/ψ and $\psi(2S)$ p_T spectra with increasing \sqrt{s} , a computation of the corresponding mean transverse momentum $\langle p_T \rangle$ and mean transverse momentum square $\langle p_T^2 \rangle$ is performed. This is achieved by fitting the J/ψ and $\psi(2S)$ p_T -differential cross sections with the following function:

$$f(p_T) = C \times \frac{p_T}{\left(1 + \left(\frac{p_T}{p_0}\right)^2\right)^n}, \quad (2)$$

with the parameters C , p_0 and n left free.

The $\langle p_T \rangle$ and $\langle p_T^2 \rangle$ are then obtained as the first and second moments of the above function in a given p_T range. The uncertainty on these quantities is evaluated by multiplying the covariance matrix of the fit on each side by the relevant Jacobian matrix, evaluated numerically and taking the square root of

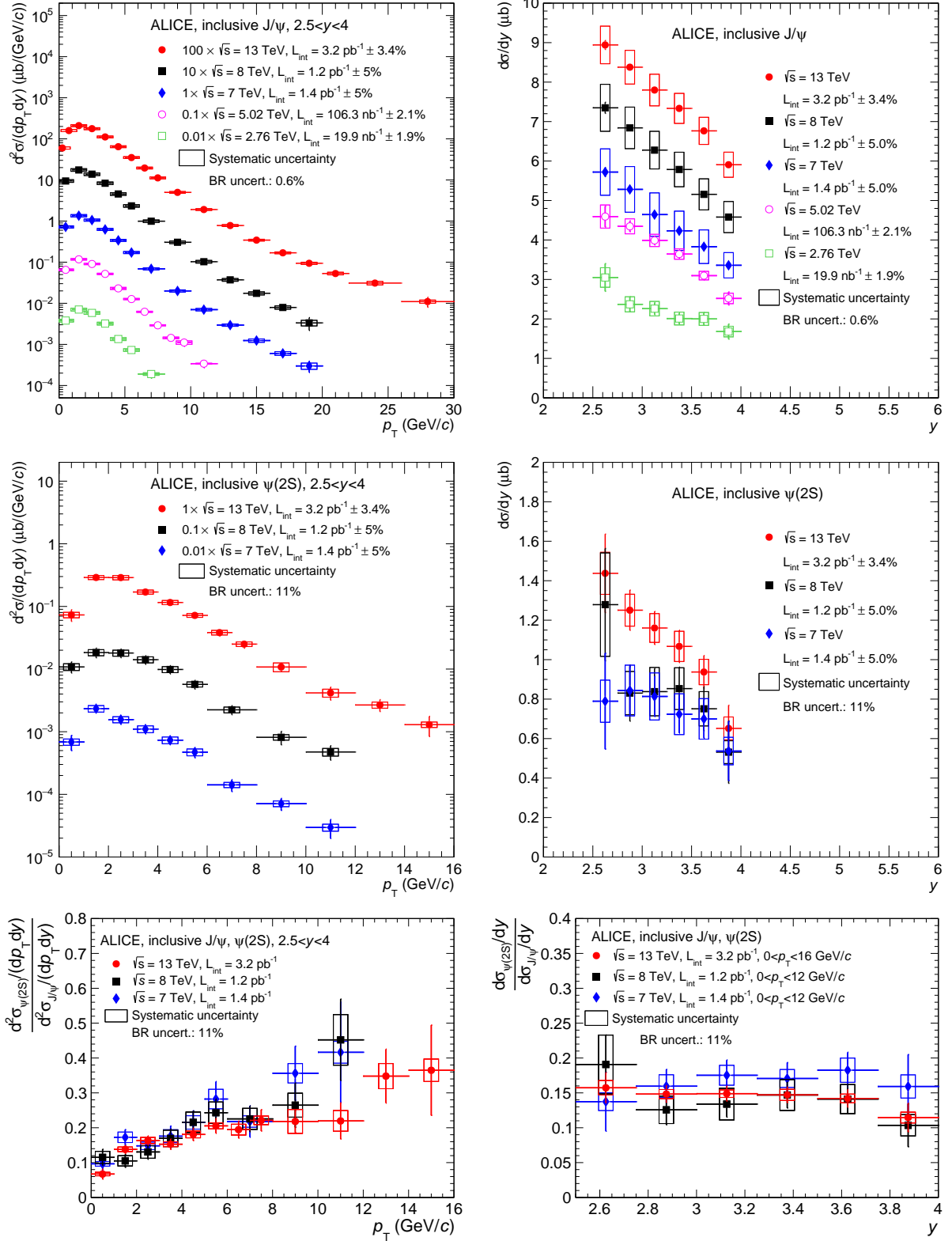


Fig. 4: (color online). Inclusive J/ψ cross sections (top), $\psi(2S)$ cross sections (middle) and $\psi(2S)$ -to- J/ψ cross section ratios (bottom) as function of p_T (left) and y (right) in pp collisions at several values of \sqrt{s} .

the result. This is performed either considering separately the statistical and uncorrelated systematic uncertainties, or by using their quadratic sum in order to obtain the corresponding statistical, systematic or total uncertainty. A similar approach was adopted in [12].

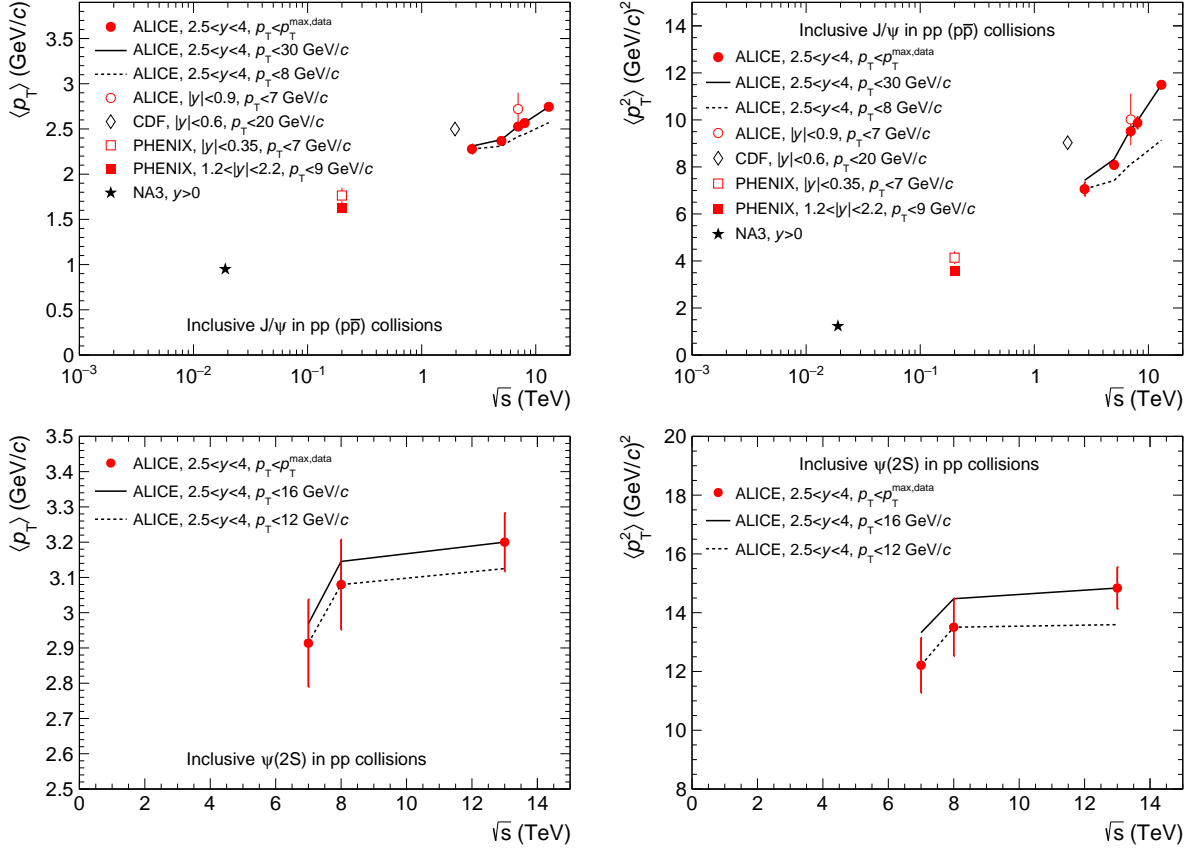


Fig. 5: $\langle p_T \rangle$ (left) and $\langle p_T^2 \rangle$ (right) as a function of \sqrt{s} for J/ψ (top) and $\psi(2S)$ (bottom). Circles correspond to ALICE data, while the other symbols correspond to measurements at lower \sqrt{s} . Vertical lines around the data points correspond to the quadratic sum of the statistical and uncorrelated systematic uncertainties. The solid lines correspond to calculating $\langle p_T \rangle$ and $\langle p_T^2 \rangle$ when extrapolating the p_T coverage to the largest available range in ALICE data ($0 < p_T < 30$ GeV/c for J/ψ and $0 < p_T < 16$ GeV/c for $\psi(2S)$), while the dashed lines correspond to truncating the data to the smallest p_T range available ($0 < p_T < 8$ GeV/c for J/ψ and $0 < p_T < 12$ GeV/c for $\psi(2S)$).

Fig. 5 shows the $\langle p_T \rangle$ (left) and $\langle p_T^2 \rangle$ (right) results for J/ψ (top) and $\psi(2S)$ (bottom). In this figure as well as in Fig. 6, the vertical lines correspond to the quadratic sum of the statistical and uncorrelated systematic uncertainties.

For J/ψ at $\sqrt{s} = 2.76$ TeV the value from [12] is used. At $\sqrt{s} = 7$ TeV the data from [13] are used instead of the result from [12] because the available integrated luminosity is much larger ($\times 90$) and the p_T reach increased from 8 to 20 GeV/c. It was checked that both results are consistent when truncated to the same p_T range. At $\sqrt{s} = 8$ TeV the data from [14] are used, while for $\sqrt{s} = 5.02$ and 13 TeV the results are from this analysis.

In the top panels of Fig. 5, ALICE measurements are compared to lower energy results from CDF [31], PHENIX [32] and NA3 [33]. A steady increase of $\langle p_T \rangle$ and $\langle p_T^2 \rangle$ is observed with increasing \sqrt{s} . This is consistent with the expected hardening of the corresponding p_T distributions. Moreover, values at mid- are systematically larger than at forward-rapidity. As discussed in [32], this observation could be attributed to an increase in the longitudinal momentum at forward-rapidity leaving less energy available in the transverse plane. The bottom panels of Fig. 5 show the corresponding measurements for $\psi(2S)$ at $\sqrt{s} = 7, 8$ and 13 TeV. An increase with \sqrt{s} is also observed similar to that of the J/ψ .

Part of the increase observed for ALICE measurements shown in all four panels of Fig. 5 is due to the

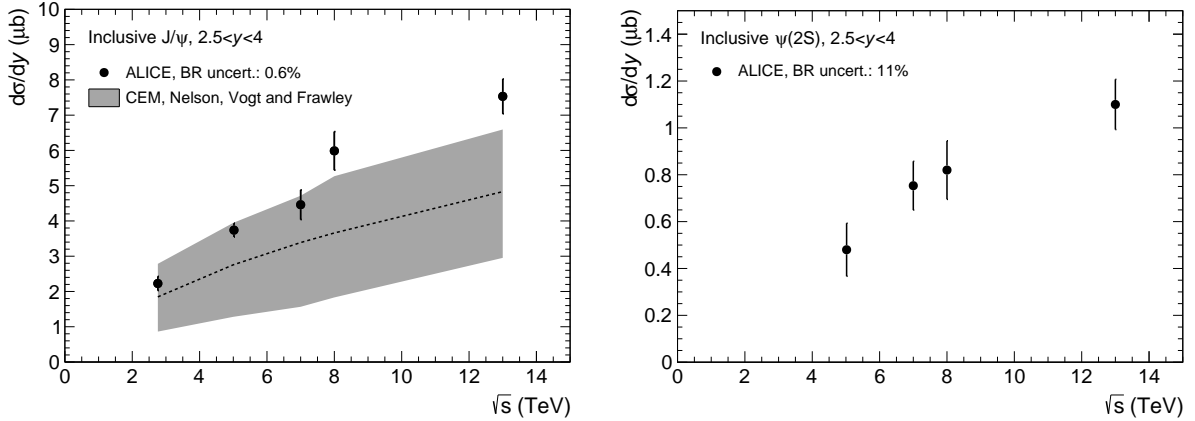


Fig. 6: J/ψ (left) and $\psi(2S)$ (right) inclusive cross section $d\sigma/dy$ as a function of \sqrt{s} . Vertical lines correspond to the quadratic sum of the statistical and uncorrelated systematic uncertainties. J/ψ cross sections are compared to a CEM calculation from [34].

fact that the p_T range used for evaluating $\langle p_T \rangle$ and $\langle p_T^2 \rangle$, chosen to be the same as in the corresponding data, also increases with \sqrt{s} . To illustrate this effect, these quantities were re-calculated either when truncating the data to the smallest available p_T range ($0 < p_T < 8$ GeV/ c for J/ψ and $0 < p_T < 12$ GeV/ c for $\psi(2S)$) or when using the fit based on Eq. 2 to extrapolate the data to the largest available range ($0 < p_T < 30$ GeV/ c for J/ψ and $0 < p_T < 16$ GeV/ c for $\psi(2S)$). The resulting values are shown in the figures as dashed lines for the truncation and solid lines for the extrapolation. In all cases the observed increasing trend still holds.

Finally, Fig. 6 shows the J/ψ (left) and $\psi(2S)$ (right) p_T - and y -integrated inclusive cross sections as a function of \sqrt{s} , measured by ALICE in the y range $2.5 < y < 4$. For both particles a steady increase of $d\sigma/dy$ is observed as a function of increasing \sqrt{s} . For the J/ψ , the cross sections are compared to a calculation done by Nelson, Vogt and Frawley in the CEM framework [34]. While the data and the model are compatible within uncertainties, the data lie on the upper side of the calculation and the difference to the central value becomes larger with increasing \sqrt{s} .

4.3 Comparisons to models

As discussed in the introduction, all ALICE J/ψ and $\psi(2S)$ measurements presented in this paper are inclusive and consist of a prompt and a non-prompt contribution. In order to compare model calculations to the data both contributions must be accounted for. This is illustrated in Fig. 7 for the J/ψ production cross section as a function of p_T in pp collisions at $\sqrt{s} = 13$ TeV.

In the left panel of Fig. 7, ALICE data are compared to three calculations: (i) in grey to a prompt J/ψ Next-to-Leading-Order (NLO) NRQCD calculation from Ma, Wang and Chao [35], (ii) in blue to a prompt J/ψ Leading Order (LO) NRQCD calculation coupled to a Color Glass Condensate (CGC) description of the low- x gluons in the proton from Ma and Venugopalan [36] and (iii) in red to a non-prompt J/ψ Fixed-Order Next-to-Leading Logarithm (FONLL) calculation by Cacciari *et al.* [37]. Both NRQCD prompt J/ψ calculations account for the decay of $\psi(2S)$ and χ_c into J/ψ .

For $p_T < 8$ GeV/ c where the contribution from non-prompt J/ψ estimated using FONLL is below 10%, the NRQCD+CGC prompt J/ψ calculation reproduces the data reasonably well. For higher p_T on the other hand, the NLO NRQCD calculation underestimates the measured cross sections and the disagreement increases with increasing p_T . This disagreement is explained by the corresponding increase of the non-prompt J/ψ contribution, which according to FONLL, becomes as high as the prompt contribution and even exceeds it for $p_T > 15$ GeV/ c . This is consistent with the measured non-prompt J/ψ fractions reported by LHCb in [11].

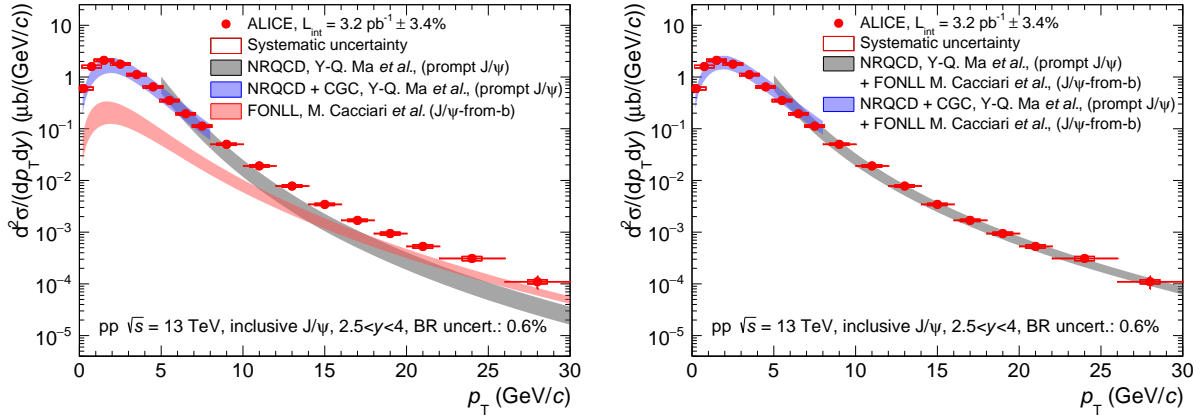


Fig. 7: (color online). Left panel: J/ψ differential cross sections (red circles) in pp collisions at $\sqrt{s} = 13$ TeV compared to NLO NRQCD (grey) [35], LO NRQCD coupled with CGC (blue) [36] and FONLL (red) [37]. Right panel: the non-prompt J/ψ contribution estimated with FONLL is summed to the two calculations for prompt J/ψ production and compared to the same data.

In the right panel of Fig. 7, the NRQCD and FONLL calculations for prompt and non-prompt J/ψ production are summed in order to obtain an *ad hoc* model of inclusive J/ψ production. The sum is performed separately for the NRQCD+CGC calculation at low p_T and the NLO NRQCD at high p_T . In both cases, the uncertainties on FONLL and NRQCD are considered as uncorrelated when calculating the uncertainty band on the sum. This is motivated by the fact that the NRQCD calculations refer to the production of charm quarks and charmed mesons, while the FONLL calculation applies to the production of beauty quarks and b -hadrons which are then decayed into J/ψ mesons. A good description of the data is obtained over the full p_T range and spanning more than four orders of magnitude in the cross sections.

The same groups have also provided NRQCD calculations for inclusive J/ψ production in pp collisions at $\sqrt{s} = 8, 7, 5.02$ and 2.76 TeV, and for $\psi(2S)$ at $\sqrt{s} = 13, 8$ and 7 TeV. These calculations are compared to ALICE measurements in Fig. 8. Also shown in this figure are comparisons from the high- p_T NLO NRQCD calculations to ALICE $\psi(2S)$ -to- J/ψ cross section ratios as a function of p_T . The motivation for showing this comparison of the cross section ratios is that many of the systematic uncertainties cancel both for the data (as discussed in Sec. 4.1) and for the theory.

Except for the cross section ratios, in all other panels the same strategy as in Fig. 7 is applied and the non-prompt contribution to inclusive charmonium production is added to the model using FONLL before comparing to the data. The FONLL+NRQCD summation is not performed for $\psi(2S)$ -to- J/ψ cross section ratios due to the added complexity introduced by the estimation of the error cancellation between the models. Moreover, the impact of the non-prompt charmonium contribution on these ratios is expected to be small because it enters both the numerator and the denominator with a similar magnitude (according to FONLL) and largely cancels out. We note that similar high- p_T NLO NRQCD calculations [38] were already compared to ALICE J/ψ and $\psi(2S)$ cross sections at $\sqrt{s} = 7$ TeV in [13], albeit with a different strategy to account for the non-prompt charmonia.

Since the NRQCD+CGC calculation from [36] extends down to zero p_T , it can be integrated over p_T and directly compared to ALICE p_T -integrated cross sections as a function of y . This calculation neglects the contribution from charmonium with $p_T > 8$ GeV/ c to the total cross section, which anyway contributes by less than 3%. The results of this comparison as a function of y are shown in Fig. 9.

Overall, a good agreement between the model and the data is observed for all measured cross sections, for both J/ψ and $\psi(2S)$ as a function of either p_T or y and for all the collision energies considered. For $\psi(2S)$ -to- J/ψ cross section ratios as a function of p_T however, the model tends to be slightly above the data especially at $\sqrt{s} = 13$ TeV. This tension appears mainly because of the error cancellation between

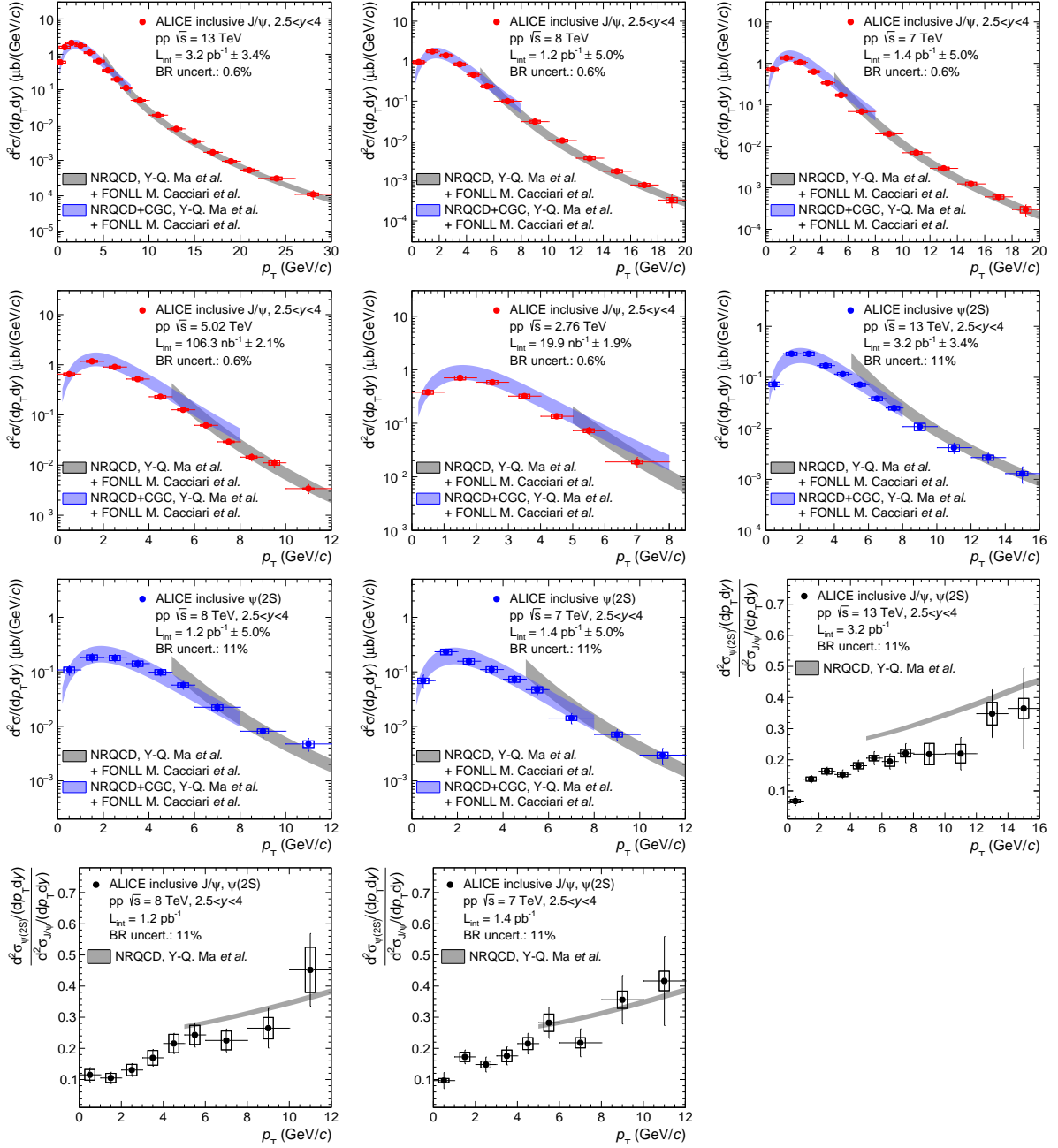


Fig. 8: (color online). Comparisons between ALICE J/ψ and $\psi(2S)$ data and summed NRQCD and FONLL model calculations from [35], [36] and [37]. The first five panels correspond to inclusive J/ψ production cross sections as a function of p_T in pp collisions at $\sqrt{s} = 13, 8, 7, 5.02$ and 2.76 TeV (red), the next three panels to inclusive $\psi(2S)$ cross sections as a function of p_T at $\sqrt{s} = 13, 8$ and 7 TeV (blue) and the last three panels to $\psi(2S)$ -to- J/ψ cross section ratios as a function of p_T at the same \sqrt{s} (black).

the uncertainties on the J/ψ and $\psi(2S)$ cross sections mentioned above.

In Fig. 10, the ALICE measurements are compared to a second set of NLO NRQCD calculations from Butenschön and Kniehl [39]. In this case only high- p_T calculations ($p_T > 3$ GeV/c) are available. The ALICE p_T -integrated cross sections as a function of y cannot be thus compared to the theory due to this p_T cut. As was the case for the comparisons shown in Figs. 8 and 9, FONLL is used to estimate the contribution from non-prompt charmonium production and added to the NRQCD calculation.

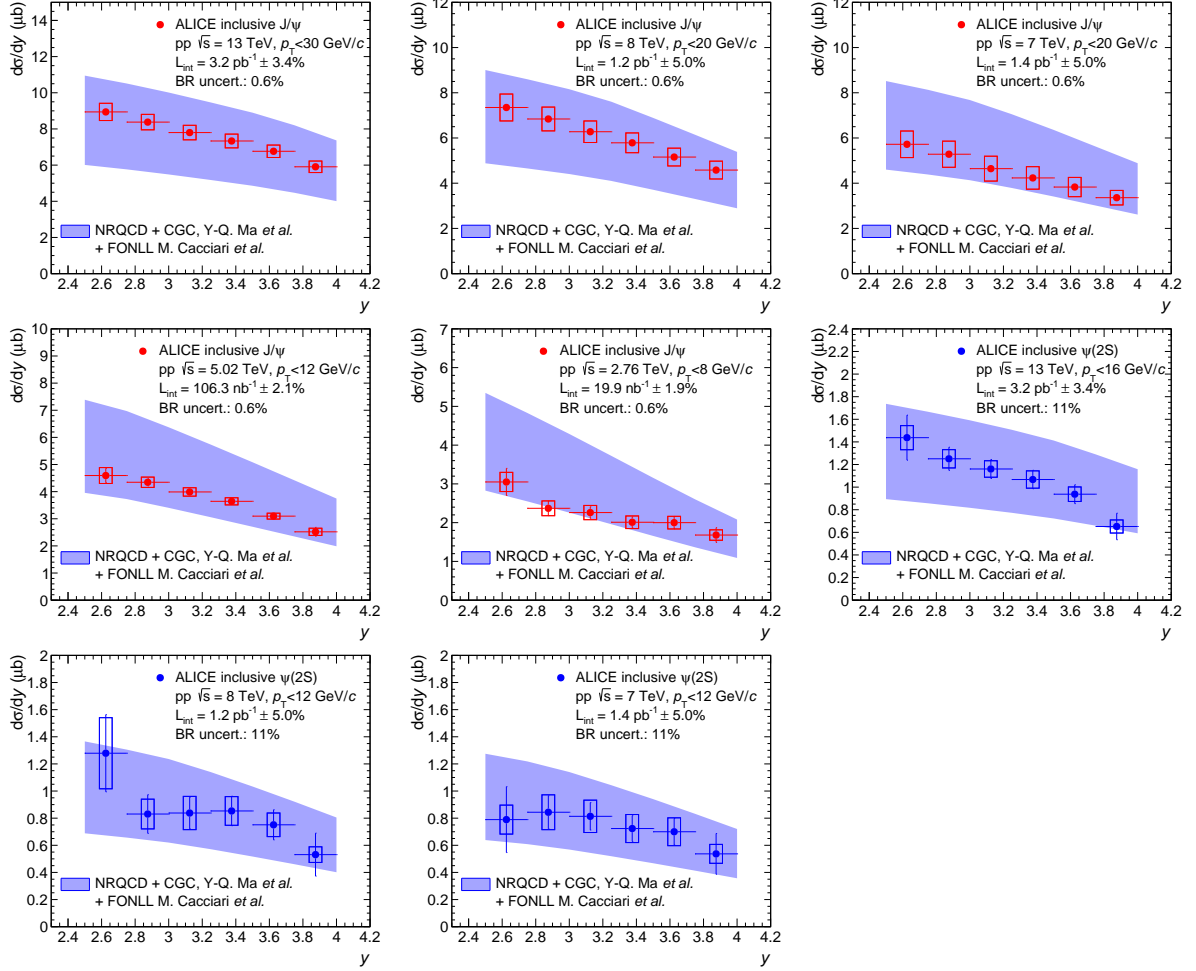


Fig. 9: (color online). Comparisons between ALICE J/ψ and $\psi(2S)$ data and summed NRQCD and FONLL model calculations from [36] and [37]. The first five panels correspond to inclusive J/ψ production cross sections as a function of y in pp collisions at $\sqrt{s} = 13, 8$ and $7, 5.02$ and 2.76 TeV (red), while the next three panels to inclusive $\psi(2S)$ cross sections as a function of y at $\sqrt{s} = 13, 8$ and 7 TeV (blue).

The two NLO NRQCD calculations from Butenschön and Kniehl (Fig. 10) and from Ma, Wang and Chao (Fig. 8) differ in the parametrization of the Long Distance Matrix Elements (LDME) used to calculate the color-octet contributions to the charmonium production cross section. The first calculation uses three matrix elements whereas the second uses only two linear combinations of these three elements. Other differences include: the data sets used to fit these matrix elements, the minimum p_T above which the calculation is applicable and the way by which contributions from χ_c and $\psi(2S)$ decays to prompt J/ψ production are accounted for.

Although the agreement between the model and the data is of similar quality in Fig. 8 and 10, some differences are visible. In particular, in Fig. 10, the calculation tends to overestimate the measured J/ψ cross sections towards high- p_T and the uncertainties are larger than in Fig. 8. The uncertainties on the $\psi(2S)$ -to- J/ψ cross section ratios are also significantly larger and consequently the agreement to the data is better. These observations are a consequence of the differences between the two calculations detailed above and in particular the fact that the fits of the LDME start at a lower p_T and include a larger number of data sets in the second case.

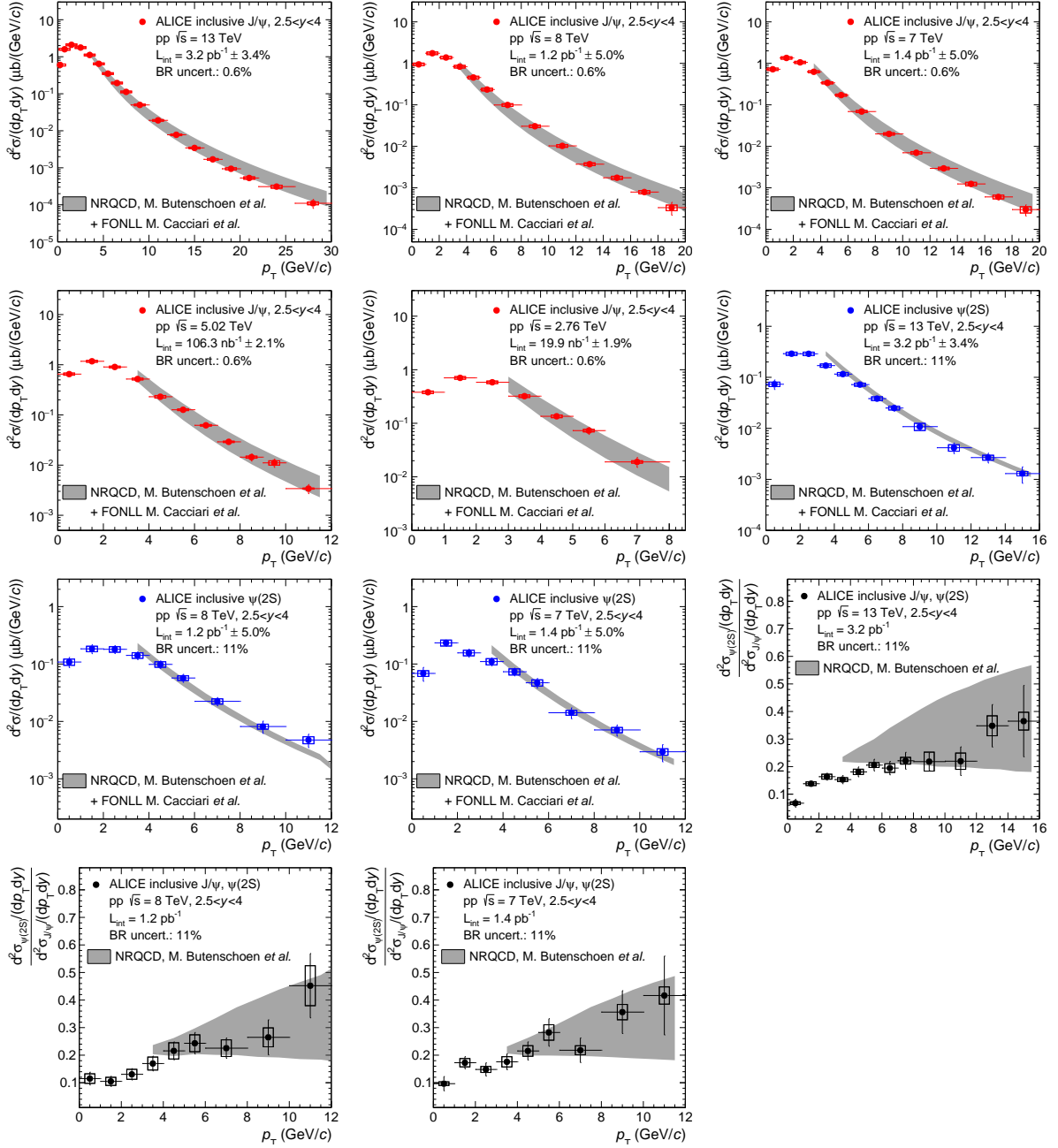


Fig. 10: (color online). Comparisons between ALICE J/ψ and $\psi(2S)$ data and summed NRQCD and FONLL model calculations from [39] and [37]. The first five panels correspond to inclusive J/ψ production cross sections as a function of p_T in pp collisions at $\sqrt{s} = 13, 8, 7, 5.02$ and 2.76 TeV (red), the next three panels to inclusive $\psi(2S)$ cross sections as a function of p_T at $\sqrt{s} = 13, 8$ and 7 TeV (blue) and the last three panels to $\psi(2S)$ -to- J/ψ cross section ratios as a function of p_T at the same \sqrt{s} (black).

5 Conclusions

The inclusive J/ψ and $\psi(2S)$ differential cross sections as well as $\psi(2S)$ -to- J/ψ cross section ratios as a function of p_T and y have been measured in pp collisions at $\sqrt{s} = 5.02$ and 13 TeV with the ALICE detector. Combined with similar measurements performed at $\sqrt{s} = 2.76$ [12], 7 [13] and 8 TeV [14], these results constitute a stringent test for models of charmonium production and allow the study of quantities such as $\langle p_T \rangle$, $\langle p_T^2 \rangle$ and p_T -integrated $d\sigma/dy$ as a function of \sqrt{s} .

The results at $\sqrt{s} = 13$ TeV significantly extend the p_T reach for both charmonium states with respect to measurements performed by ALICE at lower energies, up to 30 GeV/c for the J/ψ and 16 GeV/c for the $\psi(2S)$. When comparing the J/ψ cross sections vs p_T to measurements at lower \sqrt{s} , a hardening of the spectra is observed with increasing collision energy. This is confirmed by measurements of the J/ψ $\langle p_T \rangle$ and $\langle p_T^2 \rangle$, while a similar trend is observed for the $\psi(2S)$. Regarding inclusive $\psi(2S)$ -to- J/ψ cross section ratios, no \sqrt{s} dependence is observed within uncertainties.

Comparisons of J/ψ and $\psi(2S)$ cross sections and cross section ratios as a function of both p_T and y to NLO NRQCD and LO NRQCD+CGC prompt-charmonium calculations have been presented for all available collision energies. Concerning the J/ψ cross section as a function of p_T , an excellent agreement is observed between data and theory, provided that the non-prompt contribution to the inclusive cross section is included using FONLL. This comparison indicates that for $p_T > 15$ GeV/c, the non-prompt contribution can reach up to 50%. An overall good agreement is also observed for $\psi(2S)$ production and for the cross sections as a function of y albeit with larger uncertainties.

With the large contribution from non-prompt J/ψ to the inclusive cross sections observed for high p_T at $\sqrt{s} = 13$ TeV, it is of relatively little interest to try to further extend the p_T reach of the inclusive measurement for understanding charmonium production. This is as long as one is not capable of separating experimentally the prompt and the non-prompt contributions and relies on models instead. This separation will become possible in ALICE starting from 2021 with the addition of the Muon Forward Tracker [40].

Acknowledgements

The ALICE Collaboration would like to thank Mathias Butenschön, Matteo Cacciari, Yan-Qing Ma and Ramona Vogt for providing the NRQCD, FONLL and CEM calculations used in this paper.

The ALICE Collaboration would like to thank all its engineers and technicians for their invaluable contributions to the construction of the experiment and the CERN accelerator teams for the outstanding performance of the LHC complex. The ALICE Collaboration gratefully acknowledges the resources and support provided by all Grid centres and the Worldwide LHC Computing Grid (WLCG) collaboration. The ALICE Collaboration acknowledges the following funding agencies for their support in building and running the ALICE detector: A. I. Alikhanyan National Science Laboratory (Yerevan Physics Institute) Foundation (ANSL), State Committee of Science and World Federation of Scientists (WFS), Armenia; Austrian Academy of Sciences and Nationalstiftung für Forschung, Technologie und Entwicklung, Austria; Ministry of Communications and High Technologies, National Nuclear Research Center, Azerbaijan; Conselho Nacional de Desenvolvimento Científico e Tecnológico (CNPq), Universidade Federal do Rio Grande do Sul (UFRGS), Financiadora de Estudos e Projetos (Finep) and Fundação de Amparo à Pesquisa do Estado de São Paulo (FAPESP), Brazil; Ministry of Science & Technology of China (MSTC), National Natural Science Foundation of China (NSFC) and Ministry of Education of China (MOEC), China; Ministry of Science, Education and Sport and Croatian Science Foundation, Croatia; Ministry of Education, Youth and Sports of the Czech Republic, Czech Republic; The Danish Council for Independent Research — Natural Sciences, the Carlsberg Foundation and Danish National Research Foundation (DNRF), Denmark; Helsinki Institute of Physics (HIP), Finland; Commissariat à l’Energie Atomique (CEA) and Institut National de Physique Nucléaire et de Physique des Particules (IN2P3) and Centre National de la Recherche Scientifique (CNRS), France; Bundesministerium für Bildung, Wissenschaft, Forschung und Technologie (BMBF) and GSI Helmholtzzentrum für Schwerionenforschung GmbH, Germany; Ministry of Education, Research and Religious Affairs, Greece; National Research, Development and Innovation Office, Hungary; Department of Atomic Energy Government of India (DAE) and Council of Scientific and Industrial Research (CSIR), New Delhi, India; Indonesian Institute of Science, Indonesia; Centro Fermi - Museo Storico della Fisica e Centro Studi e Ricerche

Enrico Fermi and Istituto Nazionale di Fisica Nucleare (INFN), Italy; Institute for Innovative Science and Technology, Nagasaki Institute of Applied Science (IIST), Japan Society for the Promotion of Science (JSPS) KAKENHI and Japanese Ministry of Education, Culture, Sports, Science and Technology (MEXT), Japan; Consejo Nacional de Ciencia (CONACYT) y Tecnología, through Fondo de Cooperación Internacional en Ciencia y Tecnología (FONCICYT) and Dirección General de Asuntos del Personal Académico (DGAPA), Mexico; Nationaal instituut voor subatomaire fysica (Nikhef), Netherlands; The Research Council of Norway, Norway; Commission on Science and Technology for Sustainable Development in the South (COMSATS), Pakistan; Pontificia Universidad Católica del Perú, Peru; Ministry of Science and Higher Education and National Science Centre, Poland; Korea Institute of Science and Technology Information and National Research Foundation of Korea (NRF), Republic of Korea; Ministry of Education and Scientific Research, Institute of Atomic Physics and Romanian National Agency for Science, Technology and Innovation, Romania; Joint Institute for Nuclear Research (JINR), Ministry of Education and Science of the Russian Federation and National Research Centre Kurchatov Institute, Russia; Ministry of Education, Science, Research and Sport of the Slovak Republic, Slovakia; National Research Foundation of South Africa, South Africa; Centro de Aplicaciones Tecnológicas y Desarrollo Nuclear (CEADEN), Cubaenergía, Cuba, Ministerio de Ciencia e Innovación and Centro de Investigaciones Energéticas, Medioambientales y Tecnológicas (CIEMAT), Spain; Swedish Research Council (VR) and Knut & Alice Wallenberg Foundation (KAW), Sweden; European Organization for Nuclear Research, Switzerland; National Science and Technology Development Agency (NSDTA), Suranaree University of Technology (SUT) and Office of the Higher Education Commission under NRU project of Thailand, Thailand; Turkish Atomic Energy Agency (TAEK), Turkey; National Academy of Sciences of Ukraine, Ukraine; Science and Technology Facilities Council (STFC), United Kingdom; National Science Foundation of the United States of America (NSF) and United States Department of Energy, Office of Nuclear Physics (DOE NP), United States of America.

References

- [1] N. Brambilla *et al.*, “Heavy quarkonium: progress, puzzles, and opportunities,” *Eur. Phys. J. C* **71** (2011) 1534, arXiv:1010.5827 [hep-ph].
- [2] A. Andronic *et al.*, “Heavy-flavour and quarkonium production in the LHC era: from protonproton to heavy-ion collisions,” *Eur. Phys. J. C* **76** no. 3, (2016) 107, arXiv:1506.03981 [nucl-ex].
- [3] H. Fritzsche, “Producing Heavy Quark Flavors in Hadronic Collisions: A Test of Quantum Chromodynamics,” *Phys. Lett.* **B67** (1977) 217–221.
- [4] J. F. Amundson, O. J. P. Eboli, E. M. Gregores, and F. Halzen, “Quantitative tests of color evaporation: Charmonium production,” *Phys. Lett.* **B390** (1997) 323–328, arXiv:hep-ph/9605295 [hep-ph].
- [5] R. Baier and R. Ruckl, “Hadronic Production of J/ψ and Upsilon: Transverse Momentum Distributions,” *Phys. Lett.* **B102** (1981) 364–370.
- [6] G. T. Bodwin, E. Braaten, and G. P. Lepage, “Rigorous QCD analysis of inclusive annihilation and production of heavy quarkonium,” *Phys. Rev.* **D51** (1995) 1125–1171, arXiv:hep-ph/9407339 [hep-ph]. [Erratum: *Phys. Rev.*D55,5853(1997)].
- [7] ALICE Collaboration, B. Abelev *et al.*, “ J/ψ polarization in pp collisions at $\sqrt{s} = 7$ TeV,” *Phys. Rev. Lett.* **108** (2012) 082001, arXiv:1111.1630 [hep-ex].
- [8] LHCb Collaboration, R. Aaij *et al.*, “Measurement of J/ψ polarization in pp collisions at $\sqrt{s} = 7$ TeV,” *Eur. Phys. J. C* **73** (2013) 2631, arXiv:1307.6379 [hep-ex].

- [9] **LHCb** Collaboration, R. Aaij *et al.*, “Measurement of $\psi(2S)$ polarisation in pp collisions at $\sqrt{s} = 7$ TeV,” *Eur. Phys. J.* **C74** no. 5, (2014) 2872, arXiv:1403.1339 [hep-ex].
- [10] **ALICE** Collaboration, J. Adam *et al.*, “ J/ψ suppression at forward rapidity in Pb-Pb collisions at $\sqrt{s_{NN}} = 5.02$ TeV,” *Phys. Lett.* **B766** (2017) 212–224, arXiv:1606.08197 [nucl-ex].
- [11] **LHCb** Collaboration, R. Aaij *et al.*, “Measurement of forward J/ψ production cross-sections in pp collisions at $\sqrt{s} = 13$ TeV,” *JHEP* **10** (2015) 172, arXiv:1509.00771 [hep-ex]. [Erratum: *JHEP*05,063(2017)].
- [12] **ALICE** Collaboration, B. Abelev *et al.*, “Inclusive J/ψ production in pp collisions at $\sqrt{s} = 2.76$ TeV,” *Phys. Lett.* **B718** (2012) 295–306, arXiv:1203.3641 [hep-ex]. [Erratum: *Phys. Lett.*B748,472(2015)].
- [13] **ALICE** Collaboration, B. B. Abelev *et al.*, “Measurement of quarkonium production at forward rapidity in pp collisions at $\sqrt{s} = 7$ TeV,” *Eur. Phys. J.* **C74** no. 8, (2014) 2974, arXiv:1403.3648 [nucl-ex].
- [14] **ALICE** Collaboration, J. Adam *et al.*, “Inclusive quarkonium production at forward rapidity in pp collisions at $\sqrt{s} = 8$ TeV,” *Eur. Phys. J.* **C76** no. 4, (2016) 184, arXiv:1509.08258 [hep-ex].
- [15] J. P. Lansberg, “ J/ψ production at $\sqrt{s}=1.96$ and 7 TeV: Color-Singlet Model, NNLO* and polarisation,” *J. Phys.* **G38** (2011) 124110, arXiv:1107.0292 [hep-ph].
- [16] **ALICE** Collaboration, K. Aamodt *et al.*, “The ALICE experiment at the CERN LHC,” *JINST* **3** (2008) S08002.
- [17] **ALICE** Collaboration, B. Abelev *et al.*, “Performance of the ALICE Experiment at the CERN LHC,” *Int. J. Mod. Phys.* **A29** (2014) 1430044, arXiv:1402.4476 [nucl-ex].
- [18] **ALICE** Collaboration, K. Aamodt *et al.*, “Rapidity and transverse momentum dependence of inclusive J/ψ production in pp collisions at $\sqrt{s} = 7$ TeV,” *Phys. Lett.* **B704** (2011) 442–455, arXiv:1105.0380 [hep-ex]. [Erratum: *Phys. Lett.*B718,692(2012)].
- [19] **ALICE** Collaboration, K. Aamodt *et al.*, “Alignment of the ALICE Inner Tracking System with cosmic-ray tracks,” *JINST* **5** (2010) P03003, arXiv:1001.0502 [physics.ins-det].
- [20] **ALICE** Collaboration, E. Abbas *et al.*, “Performance of the ALICE VZERO system,” *JINST* **8** (2013) P10016, arXiv:1306.3130 [nucl-ex].
- [21] M. Bondila *et al.*, “ALICE T0 detector,” *IEEE Trans. Nucl. Sci.* **52** (2005) 1705–1711.
- [22] **ALICE** Collaboration, F. Bossù, M. Gagliardi, and M. Marchisone, “Performance of the RPC-based ALICE muon trigger system at the LHC,” *J. Instrum.* **7** no. 12, (2012) T12002. <http://stacks.iop.org/1748-0221/7/i=12/a=T12002>.
- [23] **ALICE** Collaboration, “ALICE luminosity determination for pp collisions at $\sqrt{s} = 13$ TeV,”. <https://cds.cern.ch/record/2160174>. ALICE-PUBLIC-2016-002.
- [24] **ALICE** Collaboration, “ALICE luminosity determination for pp collisions at $\sqrt{s} = 5$ TeV,”. <https://cds.cern.ch/record/2202638>. ALICE-PUBLIC-2016-005.
- [25] S. van der Meer, “Calibration of the Effective Beam Height in the ISR,” *CERN-ISR-PO-68-31* (1968). <https://cds.cern.ch/record/296752>.
- [26] **Particle Data Group** Collaboration, C. Patrignani *et al.*, “Review of Particle Physics,” *Chin. Phys.* **C40** no. 10, (2016) 100001.

- [27] ALICE Collaboration, “Quarkonium signal extraction in ALICE,” <https://cds.cern.ch/record/2060096>. ALICE-PUBLIC-2015-006.
- [28] D. J. Lange, “The EvtGen particle decay simulation package,” *Nucl. Instrum. Meth.* **A462** (2001) 152–155.
- [29] E. Barberio, B. van Eijk, and Z. Was, “PHOTOS: A Universal Monte Carlo for QED radiative corrections in decays,” *Comput. Phys. Commun.* **66** (1991) 115–128.
- [30] GEANT Collaboration, “Detector description and simulation tool, CERN Program Library Long Write-up W5013, CERN Geneva,”.
- [31] CDF Collaboration, D. Acosta *et al.*, “Measurement of the J/ψ meson and b -hadron production cross sections in $p\bar{p}$ collisions at $\sqrt{s} = 1960$ GeV,” *Phys. Rev.* **D71** (2005) 032001, [arXiv:hep-ex/0412071](https://arxiv.org/abs/hep-ex/0412071) [hep-ex].
- [32] PHENIX Collaboration, A. Adare *et al.*, “ J/ψ production versus transverse momentum and rapidity in $p + p$ collisions at $\sqrt{s} = 200$ GeV,” *Phys. Rev. Lett.* **98** (2007) 232002, [arXiv:hep-ex/0611020](https://arxiv.org/abs/hep-ex/0611020) [hep-ex].
- [33] NA3 Collaboration, J. Badier *et al.*, “Experimental J/ψ Hadronic Production from 150 GeV/c to 280 GeV/c,” *Z. Phys.* **C20** (1983) 101.
- [34] R. E. Nelson, R. Vogt, and A. D. Frawley, “Narrowing the uncertainty on the total charm cross section and its effect on the J/ψ cross section,” *Phys. Rev.* **C87** no. 1, (2013) 014908, [arXiv:1210.4610](https://arxiv.org/abs/1210.4610) [hep-ph].
- [35] Y.-Q. Ma, K. Wang, and K.-T. Chao, “ $J/\psi(\psi')$ production at the Tevatron and LHC at $\mathcal{O}(\alpha_s^4 v^4)$ in nonrelativistic QCD,” *Phys. Rev. Lett.* **106** (2011) 042002, [arXiv:1009.3655](https://arxiv.org/abs/1009.3655) [hep-ph].
- [36] Y.-Q. Ma and R. Venugopalan, “Comprehensive Description of J/ψ Production in Proton-Proton Collisions at Collider Energies,” *Phys. Rev. Lett.* **113** no. 19, (2014) 192301, [arXiv:1408.4075](https://arxiv.org/abs/1408.4075) [hep-ph].
- [37] M. Cacciari, S. Frixione, N. Houdeau, M. L. Mangano, P. Nason, and G. Ridolfi, “Theoretical predictions for charm and bottom production at the LHC,” *JHEP* **10** (2012) 137, [arXiv:1205.6344](https://arxiv.org/abs/1205.6344) [hep-ph].
- [38] Y.-Q. Ma, K. Wang, and K.-T. Chao, “A complete NLO calculation of the J/ψ and ψ' production at hadron colliders,” *Phys. Rev.* **D84** (2011) 114001, [arXiv:1012.1030](https://arxiv.org/abs/1012.1030) [hep-ph].
- [39] M. Butenschoen and B. A. Kniehl, “Reconciling J/ψ production at HERA, RHIC, Tevatron, and LHC with NRQCD factorization at next-to-leading order,” *Phys. Rev. Lett.* **106** (2011) 022003, [arXiv:1009.5662](https://arxiv.org/abs/1009.5662) [hep-ph].
- [40] ALICE Collaboration, “Technical Design Report for the Muon Forward Tracker,” Tech. Rep. CERN-LHCC-2015-001. ALICE-TDR-018, Jan, 2015. <https://cds.cern.ch/record/1981898>.

A The ALICE Collaboration

S. Acharya¹³⁹, D. Adamová⁸⁷, M.M. Aggarwal⁹¹, G. Aglieri Rinella³⁴, M. Agnello³⁰, N. Agrawal⁴⁷, Z. Ahammed¹³⁹, N. Ahmad¹⁷, S.U. Ahn⁶⁹, S. Aiola¹⁴³, A. Akindinov⁵⁴, S.N. Alam¹³⁹, D.S.D. Albuquerque¹²⁴, D. Aleksandrov⁸³, B. Alessandro¹¹³, D. Alexandre¹⁰⁴, R. Alfaro Molina⁶⁴, A. Alici^{26,12,107}, A. Alkin³, J. Alme²¹, T. Alt⁴¹, I. Altsybeev¹³⁸, C. Alves Garcia Prado¹²³, M. An⁷, C. Andrei⁸⁰, H.A. Andrews¹⁰⁴, A. Andronic¹⁰⁰, V. Anguelov⁹⁶, C. Anson⁹⁰, T. Antičić¹⁰¹, F. Antinori¹¹⁰, P. Antonioli¹⁰⁷, R. Anwar¹²⁶, L. Aphecetche¹¹⁶, H. Appelshäuser⁶⁰, S. Arcelli²⁶, R. Arnaldi¹¹³, O.W. Arnold^{97,35}, I.C. Arsene²⁰, M. Arslanodk⁶⁰, B. Audurier¹¹⁶, A. Augustinus³⁴, R. Auerbeck¹⁰⁰, M.D. Azmi¹⁷, A. Badalà¹⁰⁹, Y.W. Baek⁶⁸, S. Bagnasco¹¹³, R. Bailhache⁶⁰, R. Bala⁹³, A. Baldisseri⁶⁵, M. Ball⁴⁴, R.C. Baral⁵⁷, A.M. Barbano²⁵, R. Barbera²⁷, F. Barile^{32,106}, L. Barioglio²⁵, G.G. Barnaföldi¹⁴², L.S. Barnby^{34,104}, V. Barret⁷¹, P. Bartalini⁷, K. Barth³⁴, J. Bartke^{120,i}, E. Bartsch⁶⁰, M. Basile²⁶, N. Bastid⁷¹, S. Basu¹³⁹, B. Bathen⁶¹, G. Batigne¹¹⁶, A. Batista Camejo⁷¹, B. Batyunya⁶⁷, P.C. Batzing²⁰, I.G. Bearden⁸⁴, H. Beck⁹⁶, C. Bedda³⁰, N.K. Behera⁵⁰, I. Belikov¹³⁵, F. Bellini²⁶, H. Bello Martinez², R. Bellwied¹²⁶, L.G.E. Beltran¹²², V. Belyaev⁷⁶, G. Bencedi¹⁴², S. Beole²⁵, A. Bercuci⁸⁰, Y. Berdnikov⁸⁹, D. Berenyi¹⁴², R.A. Bertens^{53,129}, D. Berzano³⁴, L. Betev³⁴, A. Bhasin⁹³, I.R. Bhat⁹³, A.K. Bhati⁹¹, B. Bhattacharjee⁴³, J. Bhom¹²⁰, L. Bianchi¹²⁶, N. Bianchi⁷³, C. Bianchin¹⁴¹, J. Bielčič³⁸, J. Bielčiková⁸⁷, A. Bilandžić^{35,97}, G. Biro¹⁴², R. Biswas⁴, S. Biswas⁴, J.T. Blair¹²¹, D. Blau⁸³, C. Blume⁶⁰, G. Boca¹³⁶, F. Bock^{75,96}, A. Bogdanov⁷⁶, L. Boldizsár¹⁴², M. Bombara³⁹, G. Bonomi¹³⁷, M. Bonora³⁴, J. Book⁶⁰, H. Borel⁶⁵, A. Borissov⁹⁹, M. Borri¹²⁸, E. Botta²⁵, C. Bourjau⁸⁴, P. Braun-Munzinger¹⁰⁰, M. Bregant¹²³, T.A. Broker⁶⁰, T.A. Browning⁹⁸, M. Broz³⁸, E.J. Brucken⁴⁵, E. Bruna¹¹³, G.E. Bruno³², D. Budnikov¹⁰², H. Buesching⁶⁰, S. Bufalino³⁰, P. Buhler¹¹⁵, S.A.I. Buitron⁶², P. Buncic³⁴, O. Busch¹³², Z. Buthelezi⁶⁶, J.B. Butt¹⁵, J.T. Buxton¹⁸, J. Cabala¹¹⁸, D. Caffarri³⁴, H. Caines¹⁴³, A. Caliva⁵³, E. Calvo Villar¹⁰⁵, P. Camerini²⁴, A.A. Capon¹¹⁵, F. Carena³⁴, W. Carena³⁴, F. Carnesecchi^{26,12}, J. Castillo Castellanos⁶⁵, A.J. Castro¹²⁹, E.A.R. Casula^{23,108}, C. Ceballos Sanchez⁹, P. Cerello¹¹³, B. Chang¹²⁷, S. Chapeland³⁴, M. Chartier¹²⁸, J.L. Charvet⁶⁵, S. Chattopadhyay¹³⁹, S. Chattopadhyay¹⁰³, A. Chauvin^{97,35}, M. Cherny⁹⁰, C. Cheshkov¹³⁴, B. Cheynis¹³⁴, V. Chibante Barroso³⁴, D.D. Chinellato¹²⁴, S. Cho⁵⁰, P. Chochula³⁴, K. Choi⁹⁹, M. Chojnacki⁸⁴, S. Choudhury¹³⁹, P. Christakoglou⁸⁵, C.H. Christensen⁸⁴, P. Christiansen³³, T. Chujo¹³², S.U. Chung⁹⁹, C. Cicalo¹⁰⁸, L. Cifarelli^{12,26}, F. Cindolo¹⁰⁷, J. Cleymans⁹², F. Colamaria³², D. Colella^{55,34}, A. Collu⁷⁵, M. Colocci²⁶, M. Concas^{113,ii}, G. Conesa Balbastre⁷², Z. Conesa del Valle⁵¹, M.E. Connors^{143,iii}, J.G. Contreras³⁸, T.M. Cormier⁸⁸, Y. Corrales Morales¹¹³, I. Cortés Maldonado², P. Cortese³¹, M.R. Cosentino¹²⁵, F. Costa³⁴, S. Costanza¹³⁶, J. Crkovská⁵¹, P. Crochet⁷¹, E. Cuautle⁶², L. Cunqueiro⁶¹, T. Dahms^{35,97}, A. Dainese¹¹⁰, M.C. Danisch⁹⁶, A. Danu⁵⁸, D. Das¹⁰³, I. Das¹⁰³, S. Das⁴, A. Dash⁸¹, S. Dash⁴⁷, S. De^{48,123}, A. De Caro²⁹, G. de Cataldo¹⁰⁶, C. de Conti¹²³, J. de Cuveland⁴¹, A. De Falco²³, D. De Gruttola^{12,29}, N. De Marco¹¹³, S. De Pasquale²⁹, R.D. De Souza¹²⁴, H.F. Degenhardt¹²³, A. Deisting^{100,96}, A. Deloff⁷⁹, C. Deplano⁸⁵, P. Dhankher⁴⁷, D. Di Bari³², A. Di Mauro³⁴, P. Di Nezza⁷³, B. Di Ruzza¹¹⁰, M.A. Diaz Corchero¹⁰, T. Dietel⁹², P. Dillenseger⁶⁰, R. Diviã³⁴, Ø. Djuvsland²¹, A. Dobrin^{58,34}, D. Domenicis Gimenez¹²³, B. Dönigus⁶⁰, O. Dordic²⁰, T. Drozhzhova⁶⁰, A.K. Dubey¹³⁹, A. Dubla¹⁰⁰, L. Ducroux¹³⁴, A.K. Duggal⁹¹, P. Dupieux⁷¹, R.J. Ehlers¹⁴³, D. Elia¹⁰⁶, E. Endress¹⁰⁵, H. Engel⁵⁹, E. Eppe¹⁴³, B. Erazmus¹¹⁶, F. Erhardt¹³³, B. Espagnon⁵¹, S. Esumi¹³², G. Eulisse³⁴, J. Eum⁹⁹, D. Evans¹⁰⁴, S. Evdokimov¹¹⁴, L. Fabbietti^{35,97}, J. Faivre⁷², A. Fantoni⁷³, M. Fasel^{88,75}, L. Feldkamp⁶¹, A. Feliciello¹¹³, G. Feofilov¹³⁸, J. Ferencei⁸⁷, A. Fernández Téllez², E.G. Ferreira¹⁶, A. Ferretti²⁵, A. Festanti²⁸, V.J.G. Feuillard^{71,65}, J. Figiel¹²⁰, M.A.S. Figueredo¹²³, S. Filchagin¹⁰², D. Finogeev⁵², F.M. Fionda²³, E.M. Fiore³², M. Floris³⁴, S. Foertsch⁶⁶, P. Foka¹⁰⁰, S. Fokin⁸³, E. Fragiaco¹¹², A. Francescon³⁴, A. Francisco¹¹⁶, U. Frankenfeld¹⁰⁰, G.G. Fronze²⁵, U. Fuchs³⁴, C. Furget⁷², A. Furs⁵², M. Fusco Girard²⁹, J.J. Gaardhøje⁸⁴, M. Gagliardi²⁵, A.M. Gago¹⁰⁵, K. Gajdosova⁸⁴, M. Gallio²⁵, C.D. Galvan¹²², P. Ganoti⁷⁸, C. Gao⁷, C. Garabatos¹⁰⁰, E. Garcia-Solis¹³, K. Garg²⁷, P. Garg⁴⁸, C. Gargiulo³⁴, P. Gasik^{97,35}, E.F. Gauger¹²¹, M.B. Gay Ducati⁶³, M. Germain¹¹⁶, P. Ghosh¹³⁹, S.K. Ghosh⁴, P. Gianotti⁷³, P. Giubellino^{113,34}, P. Giubilato²⁸, E. Gladysz-Dziadus¹²⁰, P. Glässel⁹⁶, D.M. Gómez Coral⁶⁴, A. Gomez Ramirez⁵⁹, A.S. Gonzalez³⁴, V. Gonzalez¹⁰, P. González-Zamora¹⁰, S. Gorbunov⁴¹, L. Görlich¹²⁰, S. Gotovac¹¹⁹, V. Grabski⁶⁴, L.K. Graczykowski¹⁴⁰, K.L. Graham¹⁰⁴, L. Greiner⁷⁵, A. Grelli⁵³, C. Grigoras³⁴, V. Grigoriev⁷⁶, A. Grigoryan¹, S. Grigoryan⁶⁷, N. Grion¹¹², J.M. Gronefeld¹⁰⁰, F. Grosa³⁰, J.F. Grosse-Oetringhaus³⁴, R. Grosso¹⁰⁰, L. Gruber¹¹⁵, F.R. Grull⁵⁹, F. Guber⁵², R. Guernane⁷², B. Guerzoni²⁶, K. Gulbrandsen⁸⁴, T. Gunji¹³¹, A. Gupta⁹³, R. Gupta⁹³, I.B. Guzman², R. Haake³⁴, C. Hadjidakis⁵¹, H. Hamagaki^{77,131}, G. Hamar¹⁴², J.C. Hamon¹³⁵, J.W. Harris¹⁴³, A. Harton¹³, D. Hatzifotiadou¹⁰⁷, S. Hayashi¹³¹, S.T. Heckel⁶⁰, E. Hellbär⁶⁰, H. Helstrup³⁶, A. Hergehelegiu⁸⁰, G. Herrera Corral¹¹, F. Herrmann⁶¹, B.A. Hess⁹⁵, K.F. Hetland³⁶, H. Hillemanns³⁴, B. Hippolyte¹³⁵, J. Hladky⁵⁶, B. Hohlweger⁹⁷, D. Horak³⁸, R. Hosokawa¹³², P. Hristov³⁴, C. Hughes¹²⁹, T.J. Humanic¹⁸, N. Hussain⁴³, T. Hussain¹⁷, D. Hutter⁴¹, D.S. Hwang¹⁹, R. Ilkaev¹⁰²,

M. Inaba¹³², M. Ippolitov^{83,76}, M. Irfan¹⁷, V. Isakov⁵², M.S. Islam⁴⁸, M. Ivanov^{34,100}, V. Ivanov⁸⁹, V. Izucheev¹¹⁴, B. Jacak⁷⁵, N. Jacazio²⁶, P.M. Jacobs⁷⁵, M.B. Jadhav⁴⁷, S. Jadlovská¹¹⁸, J. Jadlovsky¹¹⁸, S. Jaelani⁵³, C. Jahnke³⁵, M.J. Jakubowska¹⁴⁰, M.A. Janik¹⁴⁰, P.H.S.Y. Jayarathna¹²⁶, C. Jena⁸¹, S. Jena¹²⁶, M. Jercic¹³³, R.T. Jimenez Bustamante¹⁰⁰, P.G. Jones¹⁰⁴, A. Jusko¹⁰⁴, P. Kalinak⁵⁵, A. Kalweit³⁴, J.H. Kang¹⁴⁴, V. Kaplin⁷⁶, S. Kar¹³⁹, A. Karasu Uysal⁷⁰, O. Karavichev⁵², T. Karavicheva⁵², L. Karayan^{100,96}, E. Karpechev⁵², U. Kebschull⁵⁹, R. Keidel¹⁴⁵, D.L.D. Keijdener⁵³, M. Keil³⁴, B. Ketzer⁴⁴, M. Mohisin Khan^{17,iv}, P. Khan¹⁰³, S.A. Khan¹³⁹, A. Khanzadeev⁸⁹, Y. Kharlov¹¹⁴, A. Khatun¹⁷, A. Khuntia⁴⁸, M.M. Kielbowicz¹²⁰, B. Kileng³⁶, D. Kim¹⁴⁴, D.W. Kim⁴², D.J. Kim¹²⁷, H. Kim¹⁴⁴, J.S. Kim⁴², J. Kim⁹⁶, M. Kim⁵⁰, M. Kim¹⁴⁴, S. Kim¹⁹, T. Kim¹⁴⁴, S. Kirsch⁴¹, I. Kisel⁴¹, S. Kiselev⁵⁴, A. Kisiel¹⁴⁰, G. Kiss¹⁴², J.L. Klay⁶, C. Klein⁶⁰, J. Klein³⁴, C. Klein-Bösing⁶¹, S. Klewin⁹⁶, A. Kluge³⁴, M.L. Knichel⁹⁶, A.G. Knospe¹²⁶, C. Kobdaj¹¹⁷, M. Kofarago³⁴, T. Kollegger¹⁰⁰, A. Kolojvari¹³⁸, V. Kondratiev¹³⁸, N. Kondratyeva⁷⁶, E. Kondratyuk¹¹⁴, A. Konevskikh⁵², M. Kopcik¹¹⁸, M. Kour⁹³, C. Kouzinopoulos³⁴, O. Kovalenko⁷⁹, V. Kovalenko¹³⁸, M. Kowalski¹²⁰, G. Koyithatta Meethalevedu⁴⁷, I. Králik⁵⁵, A. Kravčáková³⁹, M. Krivda^{55,104}, F. Krizek⁸⁷, E. Kryshen⁸⁹, M. Krzewicki⁴¹, A.M. Kubera¹⁸, V. Kučera⁸⁷, C. Kuhn¹³⁵, P.G. Kuijer⁸⁵, A. Kumar⁹³, J. Kumar⁴⁷, L. Kumar⁹¹, S. Kumar⁴⁷, S. Kundu⁸¹, P. Kurashvili⁷⁹, A. Kurepin⁵², A.B. Kurepin⁵², A. Kuryakin¹⁰², S. Kushpil⁸⁷, M.J. Kweon⁵⁰, Y. Kwon¹⁴⁴, S.L. La Pointe⁴¹, P. La Rocca²⁷, C. Lagana Fernandes¹²³, I. Lakomov³⁴, R. Langoy⁴⁰, K. Lapidus¹⁴³, C. Lara⁵⁹, A. Lardeux^{20,65}, A. Lattuca²⁵, E. Laudi³⁴, R. Lavicka³⁸, L. Lazaridis³⁴, R. Lea²⁴, L. Leardini⁹⁶, S. Lee¹⁴⁴, F. Lehas⁸⁵, S. Lehner¹¹⁵, J. Lehrbach⁴¹, R.C. Lemmon⁸⁶, V. Lenti¹⁰⁶, E. Leogrande⁵³, I. León Monzón¹²², P. Lévai¹⁴², S. Li⁷, X. Li¹⁴, J. Lien⁴⁰, R. Lietava¹⁰⁴, S. Lindal²⁰, V. Lindenstruth⁴¹, C. Lippmann¹⁰⁰, M.A. Lisa¹⁸, V. Litichevskiy⁴⁵, H.M. Ljunggren³³, W.J. Llope¹⁴¹, D.F. Lodato⁵³, P.I. Loenne²¹, V. Loginov⁷⁶, C. Loizides⁷⁵, P. Loncar¹¹⁹, X. Lopez⁷¹, E. López Torres⁹, A. Lowe¹⁴², P. Luetig⁶⁰, M. Lunardon²⁸, G. Luparello²⁴, M. Lupi³⁴, T.H. Lutz¹⁴³, A. Maevskaya⁵², M. Mager³⁴, S. Mahajan⁹³, S.M. Mahmood²⁰, A. Maire¹³⁵, R.D. Majka¹⁴³, M. Malaev⁸⁹, I. Maldonado Cervantes⁶², L. Malinina^{67,v}, D. Mal'Kevich⁵⁴, P. Malzacher¹⁰⁰, A. Mamonov¹⁰², V. Manko⁸³, F. Manso⁷¹, V. Manzari¹⁰⁶, Y. Mao⁷, M. Marchisone^{130,66}, J. Mareš⁵⁶, G.V. Margagliotti²⁴, A. Margotti¹⁰⁷, J. Margutti⁵³, A. Marín¹⁰⁰, C. Markert¹²¹, M. Marquard⁶⁰, N.A. Martin¹⁰⁰, P. Martinengo³⁴, J.A.L. Martínez⁵⁹, M.I. Martínez², G. Martínez García¹¹⁶, M. Martínez Pedreira³⁴, A. Mas¹²³, S. Masciocchi¹⁰⁰, M. Maserà²⁵, A. Masoni¹⁰⁸, A. Mastroserio³², A.M. Mathis^{97,35}, A. Matyja^{120,129}, C. Mayer¹²⁰, J. Mazer¹²⁹, M. Mazzilli³², M.A. Mazzoni¹¹¹, F. Meddi²², Y. Melikyan⁷⁶, A. Menchaca-Rocha⁶⁴, E. Meninno²⁹, J. Mercado Pérez⁹⁶, M. Meres³⁷, S. Mhlanga⁹², Y. Miake¹³², M.M. Mieskolainen⁴⁵, D.L. Mihaylov⁹⁷, K. Mikhaylov^{54,67}, L. Milano⁷⁵, J. Milosevic²⁰, A. Mischke⁵³, A.N. Mishra⁴⁸, D. Miśkowiec¹⁰⁰, J. Mitra¹³⁹, C.M. Mitu⁵⁸, N. Mohammadi⁵³, B. Mohanty⁸¹, E. Montes¹⁰, D.A. Moreira De Godoy⁶¹, L.A.P. Moreno², S. Moretto²⁸, A. Morreale¹¹⁶, A. Morsch³⁴, V. Muccifora⁷³, E. Mudnic¹¹⁹, D. Mühlheim⁶¹, S. Muhuri¹³⁹, M. Mukherjee^{139,4}, J.D. Mulligan¹⁴³, M.G. Munhoz¹²³, K. Munning⁴⁴, R.H. Munzer⁶⁰, H. Murakami¹³¹, S. Murray⁶⁶, L. Musa³⁴, J. Musinsky⁵⁵, C.J. Myers¹²⁶, B. Naik⁴⁷, R. Nair⁷⁹, B.K. Nandi⁴⁷, R. Nania¹⁰⁷, E. Nappi¹⁰⁶, M.U. Naru¹⁵, H. Natal da Luz¹²³, C. Natrass¹²⁹, S.R. Navarro², K. Nayak⁸¹, R. Nayak⁴⁷, T.K. Nayak¹³⁹, S. Nazarenko¹⁰², A. Nedosekin⁵⁴, R.A. Negrao De Oliveira³⁴, L. Nellen⁶², S.V. Nesbo³⁶, F. Ng¹²⁶, M. Nicassio¹⁰⁰, M. Niculescu⁵⁸, J. Niedziela³⁴, B.S. Nielsen⁸⁴, S. Nikolaev⁸³, S. Nikulin⁸³, V. Nikulin⁸⁹, F. Noferini^{107,12}, P. Nomokonov⁶⁷, G. Nooren⁵³, J.C.C. Noris², J. Norman¹²⁸, A. Nyanin⁸³, J. Nystrand²¹, H. Oeschler^{96,i}, S. Oh¹⁴³, A. Ohlson^{96,34}, T. Okubo⁴⁶, L. Olah¹⁴², J. Oleniacz¹⁴⁰, A.C. Oliveira Da Silva¹²³, M.H. Oliver¹⁴³, J. Onderwaater¹⁰⁰, C. Oppedisano¹¹³, R. Orava⁴⁵, M. Oravec¹¹⁸, A. Ortiz Velasquez⁶², A. Oskarsson³³, J. Otwinowski¹²⁰, K. Oyama⁷⁷, Y. Pachmayer⁹⁶, V. Pacik⁸⁴, D. Pagano¹³⁷, P. Pagano²⁹, G. Paic⁶², P. Palni⁷, J. Pan¹⁴¹, A.K. Pandey⁴⁷, S. Panebianco⁶⁵, V. Papikyan¹, G.S. Pappalardo¹⁰⁹, P. Pareek⁴⁸, J. Park⁵⁰, W.J. Park¹⁰⁰, S. Parmar⁹¹, A. Passfeld⁶¹, S.P. Pathak¹²⁶, V. Paticchio¹⁰⁶, R.N. Patra¹³⁹, B. Paul¹¹³, H. Pei⁷, T. Peitzmann⁵³, X. Peng⁷, L.G. Pereira⁶³, H. Pereira Da Costa⁶⁵, D. Peresunko^{83,76}, E. Perez Lezama⁶⁰, V. Peskov⁶⁰, Y. Pestov⁵, V. Petráček³⁸, V. Petrov¹¹⁴, M. Petrovici⁸⁰, C. Petta²⁷, R.P. Pezzi⁶³, S. Piano¹¹², M. Pikna³⁷, P. Pillot¹¹⁶, L.O.D.L. Pimentel⁸⁴, O. Pinazza^{107,34}, L. Pinsky¹²⁶, D.B. Piyarathna¹²⁶, M. Płoskoń⁷⁵, M. Planinic¹³³, J. Pluta¹⁴⁰, S. Pochybova¹⁴², P.L.M. Podesta-Lerma¹²², M.G. Poghosyan⁸⁸, B. Polichtchouk¹¹⁴, N. Poljak¹³³, W. Poonsawat¹¹⁷, A. Pop⁸⁰, H. Poppenborg⁶¹, S. Porteboeuf-Houssais⁷¹, J. Porter⁷⁵, J. Pospisil⁸⁷, V. Pozdniakov⁶⁷, S.K. Prasad⁴, R. Preghenella^{34,107}, F. Prino¹¹³, C.A. Pruneau¹⁴¹, I. Pshenichnov⁵², M. Puccio²⁵, G. Puddu²³, P. Pujahari¹⁴¹, V. Punin¹⁰², J. Putschke¹⁴¹, H. Qvigstad²⁰, A. Rachevski¹¹², S. Raha⁴, S. Rajput⁹³, J. Rak¹²⁷, A. Rakotozafindrabe⁶⁵, L. Ramello³¹, F. Rami¹³⁵, D.B. Rana¹²⁶, R. Raniwala⁹⁴, S. Raniwala⁹⁴, S.S. Räsänen⁴⁵, B.T. Rascanu⁶⁰, D. Rathee⁹¹, V. Ratza⁴⁴, I. Ravasenga³⁰, K.F. Read^{88,129}, K. Redlich⁷⁹, A. Rehman²¹, P. Reichelt⁶⁰, F. Reidt³⁴, X. Ren⁷, R. Renfordt⁶⁰, A.R. Reolon⁷³, A. Reshetin⁵², K. Reygers⁹⁶, V. Riabov⁸⁹, R.A. Ricci⁷⁴, T. Richert^{53,33}, M. Richter²⁰, P. Riedler³⁴, W. Riegler³⁴, F. Riggi²⁷, C. Ristea⁵⁸, M. Rodríguez Cahuantzi², K. Røed²⁰, E. Rogochaya⁶⁷, D. Rohr⁴¹, D. Röhrich²¹, P.S. Rokita¹⁴⁰,

F. Ronchetti^{34,73}, L. Ronflette¹¹⁶, P. Rosnet⁷¹, A. Rossi²⁸, A. Rotondi¹³⁶, F. Roukoutakis⁷⁸, A. Roy⁴⁸, C. Roy¹³⁵, P. Roy¹⁰³, A.J. Rubio Montero¹⁰, O.V. Rueda⁶², R. Rui²⁴, R. Russo²⁵, A. Rustamov⁸², E. Ryabinkin⁸³, Y. Ryabov⁸⁹, A. Rybicki¹²⁰, S. Saarinen⁴⁵, S. Sadhu¹³⁹, S. Sadovsky¹¹⁴, K. Šafařík³⁴, S.K. Saha¹³⁹, B. Sahlmuller⁶⁰, B. Sahoo⁴⁷, P. Sahoo⁴⁸, R. Sahoo⁴⁸, S. Sahoo⁵⁷, P.K. Sahu⁵⁷, J. Saini¹³⁹, S. Sakai^{73,132}, M.A. Saleh¹⁴¹, J. Salzwedel¹⁸, S. Sambyal⁹³, V. Samsonov^{76,89}, A. Sandoval⁶⁴, D. Sarkar¹³⁹, N. Sarkar¹³⁹, P. Sarma⁴³, M.H.P. Sas⁵³, E. Scapparone¹⁰⁷, F. Scarlassara²⁸, R.P. Scharenberg⁹⁸, H.S. Scheid⁶⁰, C. Schiaua⁸⁰, R. Schicker⁹⁶, C. Schmidt¹⁰⁰, H.R. Schmidt⁹⁵, M.O. Schmidt⁹⁶, M. Schmidt⁹⁵, S. Schuchmann⁶⁰, J. Schukraft³⁴, Y. Schutz^{116,135,34}, K. Schwarz¹⁰⁰, K. Schweda¹⁰⁰, G. Scioli²⁶, E. Scomparin¹¹³, R. Scott¹²⁹, M. Šefčík³⁹, J.E. Seger⁹⁰, Y. Sekiguchi¹³¹, D. Sekihata⁴⁶, I. Selyuzhenkov¹⁰⁰, K. Senosi⁶⁶, S. Senyukov^{3,135,34}, E. Serradilla^{64,10}, P. Sett⁴⁷, A. Sevcenco⁵⁸, A. Shabanov⁵², A. Shabetai¹¹⁶, O. Shadura³, R. Shahoyan³⁴, A. Shangaraev¹¹⁴, A. Sharma⁹¹, A. Sharma⁹³, M. Sharma⁹³, M. Sharma⁹³, N. Sharma^{129,91}, A.I. Sheikh¹³⁹, K. Shigaki⁴⁶, Q. Shou⁷, K. Shtejer^{25,9}, Y. Sibirjak⁸³, S. Siddhanta¹⁰⁸, K.M. Sielewicz³⁴, T. Siemiarczuk⁷⁹, D. Silvermyr³³, C. Silvestre⁷², G. Simatovic¹³³, G. Simonetti³⁴, R. Singaraju¹³⁹, R. Singh⁸¹, V. Singhal¹³⁹, T. Sinha¹⁰³, B. Sitar³⁷, M. Sitta³¹, T.B. Skaali²⁰, M. Slupecki¹²⁷, N. Smirnov¹⁴³, R.J.M. Snellings⁵³, T.W. Snellman¹²⁷, J. Song⁹⁹, M. Song¹⁴⁴, F. Soramel²⁸, S. Sorensen¹²⁹, F. Sozzi¹⁰⁰, E. Spiriti⁷³, I. Sputowska¹²⁰, B.K. Srivastava⁹⁸, J. Stachel⁹⁶, I. Stan⁵⁸, P. Stankus⁸⁸, E. Stenlund³³, J.H. Stiller⁹⁶, D. Stocco¹¹⁶, P. Strmen³⁷, A.A.P. Suaide¹²³, T. Sugitate⁴⁶, C. Suire⁵¹, M. Suleymanov¹⁵, M. Suljic²⁴, R. Sultanov⁵⁴, M. Šumbera⁸⁷, S. Sumowidagdo⁴⁹, K. Suzuki¹¹⁵, S. Swain⁵⁷, A. Szabo³⁷, I. Szarka³⁷, A. Szczepankiewicz¹⁴⁰, M. Szymanski¹⁴⁰, U. Tabassam¹⁵, J. Takahashi¹²⁴, G.J. Tambave²¹, N. Tanaka¹³², M. Tarhini⁵¹, M. Tariq¹⁷, M.G. Tarzila⁸⁰, A. Tauro³⁴, G. Tejada Muñoz², A. Telesca³⁴, K. Terasaki¹³¹, C. Terrevoli²⁸, B. Teyssier¹³⁴, D. Thakur⁴⁸, S. Thakur¹³⁹, D. Thomas¹²¹, R. Tieulent¹³⁴, A. Tikhonov⁵², A.R. Timmins¹²⁶, A. Toia⁶⁰, S. Tripathy⁴⁸, S. Trogolo²⁵, G. Trombetta³², V. Trubnikov³, W.H. Trzaska¹²⁷, B.A. Trzeciak⁵³, T. Tsuji¹³¹, A. Tumkin¹⁰², R. Turrisi¹¹⁰, T.S. Tveter²⁰, K. Ullaland²¹, E.N. Umaka¹²⁶, A. Uras¹³⁴, G.L. Usai²³, A. Utrobicic¹³³, M. Vala^{118,55}, J. Van Der Maarel⁵³, J.W. Van Hoorne³⁴, M. van Leeuwen⁵³, T. Vanat⁸⁷, P. Vande Vyvre³⁴, D. Varga¹⁴², A. Vargas², M. Vargyas¹²⁷, R. Varma⁴⁷, M. Vasileiou⁷⁸, A. Vasiliev⁸³, A. Vauthier⁷², O. Vázquez Doce^{97,35}, V. Vechernin¹³⁸, A.M. Veen⁵³, A. Velure²¹, E. Vercellin²⁵, S. Vergara Limón², R. Vernet⁸, R. Vértesi¹⁴², L. Vickovic¹¹⁹, S. Vigolo⁵³, J. Viinikainen¹²⁷, Z. Vilakazi¹³⁰, O. Villalobos Baillie¹⁰⁴, A. Villatoro Tello², A. Vinogradov⁸³, L. Vinogradov¹³⁸, T. Virgili²⁹, V. Vislavicius³³, A. Vodopyanov⁶⁷, M.A. Völkl⁹⁶, K. Voloshin⁵⁴, S.A. Voloshin¹⁴¹, G. Volpe³², B. von Haller³⁴, I. Vorobyev^{97,35}, D. Voscek¹¹⁸, D. Vranic^{34,100}, J. Vrláková³⁹, B. Wagner²¹, J. Wagner¹⁰⁰, H. Wang⁵³, M. Wang⁷, D. Watanabe¹³², Y. Watanabe¹³¹, M. Weber¹¹⁵, S.G. Weber¹⁰⁰, D.F. Weiser⁹⁶, J.P. Wessels⁶¹, U. Westerhoff⁶¹, A.M. Whitehead⁹², J. Wiechula⁶⁰, J. Wikne²⁰, G. Wilk⁷⁹, J. Wilkinson⁹⁶, G.A. Willems⁶¹, M.C.S. Williams¹⁰⁷, B. Windelband⁹⁶, W.E. Witt¹²⁹, S. Yalcin⁷⁰, P. Yang⁷, S. Yano⁴⁶, Z. Yin⁷, H. Yokoyama^{132,72}, I.-K. Yoo^{34,99}, J.H. Yoon⁵⁰, V. Yurchenko³, V. Zaccolo^{113,84}, A. Zaman¹⁵, C. Zampolli³⁴, H.J.C. Zanolini¹²³, N. Zardoshti¹⁰⁴, A. Zarochentsev¹³⁸, P. Závada⁵⁶, N. Zaviyalov¹⁰², H. Zbroszczyk¹⁴⁰, M. Zhalov⁸⁹, H. Zhang^{21,7}, X. Zhang⁷, Y. Zhang⁷, C. Zhang⁵³, Z. Zhang⁷, C. Zhao²⁰, N. Zhigareva⁵⁴, D. Zhou⁷, Y. Zhou⁸⁴, Z. Zhou²¹, H. Zhu^{21,7}, J. Zhu^{7,116}, X. Zhu⁷, A. Zichichi^{26,12}, A. Zimmermann⁹⁶, M.B. Zimmermann^{34,61}, S. Zimmermann¹¹⁵, G. Zinovjev³, J. Zmeskal¹¹⁵

Affiliation notes

- ⁱ Deceased
- ⁱⁱ Also at: Dipartimento DET del Politecnico di Torino, Turin, Italy
- ⁱⁱⁱ Also at: Georgia State University, Atlanta, Georgia, United States
- ^{iv} Also at: Also at Department of Applied Physics, Aligarh Muslim University, Aligarh, India
- ^v Also at: M.V. Lomonosov Moscow State University, D.V. Skobeltsyn Institute of Nuclear, Physics, Moscow, Russia

Collaboration Institutes

- ¹A.I. Alikhanyan National Science Laboratory (Yerevan Physics Institute) Foundation, Yerevan, Armenia
- ²Benemérita Universidad Autónoma de Puebla, Puebla, Mexico
- ³Bogolyubov Institute for Theoretical Physics, Kiev, Ukraine
- ⁴Bose Institute, Department of Physics and Centre for Astroparticle Physics and Space Science (CAPSS), Kolkata, India
- ⁵Budker Institute for Nuclear Physics, Novosibirsk, Russia

- ⁶California Polytechnic State University, San Luis Obispo, California, United States
⁷Central China Normal University, Wuhan, China
⁸Centre de Calcul de l'IN2P3, Villeurbanne, Lyon, France
⁹Centro de Aplicaciones Tecnológicas y Desarrollo Nuclear (CEADEN), Havana, Cuba
¹⁰Centro de Investigaciones Energéticas Medioambientales y Tecnológicas (CIEMAT), Madrid, Spain
¹¹Centro de Investigación y de Estudios Avanzados (CINVESTAV), Mexico City and Mérida, Mexico
¹²Centro Fermi - Museo Storico della Fisica e Centro Studi e Ricerche "Enrico Fermi", Rome, Italy
¹³Chicago State University, Chicago, Illinois, United States
¹⁴China Institute of Atomic Energy, Beijing, China
¹⁵COMSATS Institute of Information Technology (CIIT), Islamabad, Pakistan
¹⁶Departamento de Física de Partículas and IGFAE, Universidad de Santiago de Compostela, Santiago de Compostela, Spain
¹⁷Department of Physics, Aligarh Muslim University, Aligarh, India
¹⁸Department of Physics, Ohio State University, Columbus, Ohio, United States
¹⁹Department of Physics, Sejong University, Seoul, South Korea
²⁰Department of Physics, University of Oslo, Oslo, Norway
²¹Department of Physics and Technology, University of Bergen, Bergen, Norway
²²Dipartimento di Fisica dell'Università 'La Sapienza' and Sezione INFN, Rome, Italy
²³Dipartimento di Fisica dell'Università and Sezione INFN, Cagliari, Italy
²⁴Dipartimento di Fisica dell'Università and Sezione INFN, Trieste, Italy
²⁵Dipartimento di Fisica dell'Università and Sezione INFN, Turin, Italy
²⁶Dipartimento di Fisica e Astronomia dell'Università and Sezione INFN, Bologna, Italy
²⁷Dipartimento di Fisica e Astronomia dell'Università and Sezione INFN, Catania, Italy
²⁸Dipartimento di Fisica e Astronomia dell'Università and Sezione INFN, Padova, Italy
²⁹Dipartimento di Fisica 'E.R. Caianiello' dell'Università and Gruppo Collegato INFN, Salerno, Italy
³⁰Dipartimento DISAT del Politecnico and Sezione INFN, Turin, Italy
³¹Dipartimento di Scienze e Innovazione Tecnologica dell'Università del Piemonte Orientale and INFN Sezione di Torino, Alessandria, Italy
³²Dipartimento Interateneo di Fisica 'M. Merlin' and Sezione INFN, Bari, Italy
³³Division of Experimental High Energy Physics, University of Lund, Lund, Sweden
³⁴European Organization for Nuclear Research (CERN), Geneva, Switzerland
³⁵Excellence Cluster Universe, Technische Universität München, Munich, Germany
³⁶Faculty of Engineering, Bergen University College, Bergen, Norway
³⁷Faculty of Mathematics, Physics and Informatics, Comenius University, Bratislava, Slovakia
³⁸Faculty of Nuclear Sciences and Physical Engineering, Czech Technical University in Prague, Prague, Czech Republic
³⁹Faculty of Science, P.J. Šafárik University, Košice, Slovakia
⁴⁰Faculty of Technology, Buskerud and Vestfold University College, Tonsberg, Norway
⁴¹Frankfurt Institute for Advanced Studies, Johann Wolfgang Goethe-Universität Frankfurt, Frankfurt, Germany
⁴²Gangneung-Wonju National University, Gangneung, South Korea
⁴³Gauhati University, Department of Physics, Guwahati, India
⁴⁴Helmholtz-Institut für Strahlen- und Kernphysik, Rheinische Friedrich-Wilhelms-Universität Bonn, Bonn, Germany
⁴⁵Helsinki Institute of Physics (HIP), Helsinki, Finland
⁴⁶Hiroshima University, Hiroshima, Japan
⁴⁷Indian Institute of Technology Bombay (IIT), Mumbai, India
⁴⁸Indian Institute of Technology Indore, Indore, India
⁴⁹Indonesian Institute of Sciences, Jakarta, Indonesia
⁵⁰Inha University, Incheon, South Korea
⁵¹Institut de Physique Nucléaire d'Orsay (IPNO), Université Paris-Sud, CNRS-IN2P3, Orsay, France
⁵²Institute for Nuclear Research, Academy of Sciences, Moscow, Russia
⁵³Institute for Subatomic Physics of Utrecht University, Utrecht, Netherlands
⁵⁴Institute for Theoretical and Experimental Physics, Moscow, Russia
⁵⁵Institute of Experimental Physics, Slovak Academy of Sciences, Košice, Slovakia
⁵⁶Institute of Physics, Academy of Sciences of the Czech Republic, Prague, Czech Republic
⁵⁷Institute of Physics, Bhubaneswar, India

- ⁵⁸Institute of Space Science (ISS), Bucharest, Romania
⁵⁹Institut für Informatik, Johann Wolfgang Goethe-Universität Frankfurt, Frankfurt, Germany
⁶⁰Institut für Kernphysik, Johann Wolfgang Goethe-Universität Frankfurt, Frankfurt, Germany
⁶¹Institut für Kernphysik, Westfälische Wilhelms-Universität Münster, Münster, Germany
⁶²Instituto de Ciencias Nucleares, Universidad Nacional Autónoma de México, Mexico City, Mexico
⁶³Instituto de Física, Universidade Federal do Rio Grande do Sul (UFRGS), Porto Alegre, Brazil
⁶⁴Instituto de Física, Universidad Nacional Autónoma de México, Mexico City, Mexico
⁶⁵IRFU, CEA, Université Paris-Saclay, F-91191 Gif-sur-Yvette, France, Saclay, France
⁶⁶iThemba LABS, National Research Foundation, Somerset West, South Africa
⁶⁷Joint Institute for Nuclear Research (JINR), Dubna, Russia
⁶⁸Konkuk University, Seoul, South Korea
⁶⁹Korea Institute of Science and Technology Information, Daejeon, South Korea
⁷⁰KTO Karatay University, Konya, Turkey
⁷¹Laboratoire de Physique Corpusculaire (LPC), Clermont Université, Université Blaise Pascal, CNRS-IN2P3, Clermont-Ferrand, France
⁷²Laboratoire de Physique Subatomique et de Cosmologie, Université Grenoble-Alpes, CNRS-IN2P3, Grenoble, France
⁷³Laboratori Nazionali di Frascati, INFN, Frascati, Italy
⁷⁴Laboratori Nazionali di Legnaro, INFN, Legnaro, Italy
⁷⁵Lawrence Berkeley National Laboratory, Berkeley, California, United States
⁷⁶Moscow Engineering Physics Institute, Moscow, Russia
⁷⁷Nagasaki Institute of Applied Science, Nagasaki, Japan
⁷⁸National and Kapodistrian University of Athens, Physics Department, Athens, Greece, Athens, Greece
⁷⁹National Centre for Nuclear Studies, Warsaw, Poland
⁸⁰National Institute for Physics and Nuclear Engineering, Bucharest, Romania
⁸¹National Institute of Science Education and Research, Bhubaneswar, India
⁸²National Nuclear Research Center, Baku, Azerbaijan
⁸³National Research Centre Kurchatov Institute, Moscow, Russia
⁸⁴Niels Bohr Institute, University of Copenhagen, Copenhagen, Denmark
⁸⁵Nikhef, Nationaal instituut voor subatomaire fysica, Amsterdam, Netherlands
⁸⁶Nuclear Physics Group, STFC Daresbury Laboratory, Daresbury, United Kingdom
⁸⁷Nuclear Physics Institute, Academy of Sciences of the Czech Republic, Řež u Prahy, Czech Republic
⁸⁸Oak Ridge National Laboratory, Oak Ridge, Tennessee, United States
⁸⁹Petersburg Nuclear Physics Institute, Gatchina, Russia
⁹⁰Physics Department, Creighton University, Omaha, Nebraska, United States
⁹¹Physics Department, Panjab University, Chandigarh, India
⁹²Physics Department, University of Cape Town, Cape Town, South Africa
⁹³Physics Department, University of Jammu, Jammu, India
⁹⁴Physics Department, University of Rajasthan, Jaipur, India
⁹⁵Physikalisches Institut, Eberhard Karls Universität Tübingen, Tübingen, Germany
⁹⁶Physikalisches Institut, Ruprecht-Karls-Universität Heidelberg, Heidelberg, Germany
⁹⁷Physik Department, Technische Universität München, Munich, Germany
⁹⁸Purdue University, West Lafayette, Indiana, United States
⁹⁹Pusan National University, Pusan, South Korea
¹⁰⁰Research Division and ExtreMe Matter Institute EMMI, GSI Helmholtzzentrum für Schwerionenforschung GmbH, Darmstadt, Germany
¹⁰¹Rudjer Bošković Institute, Zagreb, Croatia
¹⁰²Russian Federal Nuclear Center (VNIIEF), Sarov, Russia
¹⁰³Saha Institute of Nuclear Physics, Kolkata, India
¹⁰⁴School of Physics and Astronomy, University of Birmingham, Birmingham, United Kingdom
¹⁰⁵Sección Física, Departamento de Ciencias, Pontificia Universidad Católica del Perú, Lima, Peru
¹⁰⁶Sezione INFN, Bari, Italy
¹⁰⁷Sezione INFN, Bologna, Italy
¹⁰⁸Sezione INFN, Cagliari, Italy
¹⁰⁹Sezione INFN, Catania, Italy
¹¹⁰Sezione INFN, Padova, Italy

- ¹¹¹Sezione INFN, Rome, Italy
- ¹¹²Sezione INFN, Trieste, Italy
- ¹¹³Sezione INFN, Turin, Italy
- ¹¹⁴SSC IHEP of NRC Kurchatov institute, Protvino, Russia
- ¹¹⁵Stefan Meyer Institut für Subatomare Physik (SMI), Vienna, Austria
- ¹¹⁶SUBATECH, IMT Atlantique, Université de Nantes, CNRS-IN2P3, Nantes, France
- ¹¹⁷Suranaree University of Technology, Nakhon Ratchasima, Thailand
- ¹¹⁸Technical University of Košice, Košice, Slovakia
- ¹¹⁹Technical University of Split FESB, Split, Croatia
- ¹²⁰The Henryk Niewodniczanski Institute of Nuclear Physics, Polish Academy of Sciences, Cracow, Poland
- ¹²¹The University of Texas at Austin, Physics Department, Austin, Texas, United States
- ¹²²Universidad Autónoma de Sinaloa, Culiacán, Mexico
- ¹²³Universidade de São Paulo (USP), São Paulo, Brazil
- ¹²⁴Universidade Estadual de Campinas (UNICAMP), Campinas, Brazil
- ¹²⁵Universidade Federal do ABC, Santo Andre, Brazil
- ¹²⁶University of Houston, Houston, Texas, United States
- ¹²⁷University of Jyväskylä, Jyväskylä, Finland
- ¹²⁸University of Liverpool, Liverpool, United Kingdom
- ¹²⁹University of Tennessee, Knoxville, Tennessee, United States
- ¹³⁰University of the Witwatersrand, Johannesburg, South Africa
- ¹³¹University of Tokyo, Tokyo, Japan
- ¹³²University of Tsukuba, Tsukuba, Japan
- ¹³³University of Zagreb, Zagreb, Croatia
- ¹³⁴Université de Lyon, Université Lyon 1, CNRS/IN2P3, IPN-Lyon, Villeurbanne, Lyon, France
- ¹³⁵Université de Strasbourg, CNRS, IPHC UMR 7178, F-67000 Strasbourg, France, Strasbourg, France
- ¹³⁶Università degli Studi di Pavia, Pavia, Italy
- ¹³⁷Università di Brescia, Brescia, Italy
- ¹³⁸V. Fock Institute for Physics, St. Petersburg State University, St. Petersburg, Russia
- ¹³⁹Variable Energy Cyclotron Centre, Kolkata, India
- ¹⁴⁰Warsaw University of Technology, Warsaw, Poland
- ¹⁴¹Wayne State University, Detroit, Michigan, United States
- ¹⁴²Wigner Research Centre for Physics, Hungarian Academy of Sciences, Budapest, Hungary
- ¹⁴³Yale University, New Haven, Connecticut, United States
- ¹⁴⁴Yonsei University, Seoul, South Korea
- ¹⁴⁵Zentrum für Technologietransfer und Telekommunikation (ZTT), Fachhochschule Worms, Worms, Germany